Journal of Palaeogeography
2015, 4(2): 167−188
DOI: 10.3724/SP.J.1261.2015.00072

Tectonopalaeogeography and palaeotectonics

Geodynamic evolution of the Earth over the Phanerozoic: Plate tectonic activity and palaeoclimatic indicators

Christian Vérard*, Cyril Hochard, Peter O. Baumgartner, Gérard M. Stampfli

Université de Lausanne (UNIL), Institut des Sciences de la Terre (ISTE), Geopolis, CH-1015 Lausanne, Switzerland

Abstract During the last decades, numerous local reconstructions based on field geology were developed at the University of Lausanne (UNIL). Team members of the UNIL participated in the elaboration of a 600 Ma to present global plate tectonic model deeply rooted in geological data, controlled by geometric and kinematic constraints and coherent with forces acting at plate boundaries.

In this paper, we compare values derived from the tectonic model (ages of oceanic floor, production and subduction rates, tectonic activity) with a combination of chemical proxies (namely CO_2, $^{87}Sr/^{86}Sr$, glaciation evidence, and sea-level variations) known to be strongly influenced by tectonics. One of the outstanding results is the observation of an overall decreasing trend in the evolution of the global tectonic activity, mean oceanic ages and plate velocities over the whole Phanerozoic. We speculate that the decreasing trend reflects the global cooling of the Earth system. Additionally, the parallel between the tectonic activity and CO_2 together with the extension of glaciations confirms the generally accepted idea of a primary control of CO_2 on climate and highlights the link between plate tectonics and CO_2 in a time scale greater than 10^7 yr. Last, the wide variations observed in the reconstructed sea-floor production rates are in contradiction with the steady-state model hypothesized by some.

Key words geodynamic, plate tectonics, plate model, Phanerozoic, palaeoclimate, CO_2, strontium, glaciation

1 Introduction

The spatial and temporal distribution of continents and oceans throughout the Phanerozoic is of major concern in a wide range of scientific studies. At the interface between the inner and the outer shells, lithospheric plates are an essential link of the global Earth system. On the one hand, palinspastic reconstructions offer an ideal framework to geological and palaeogeographical studies; on the other hand, they can be used as boundary conditions in palaeoclimatic, palaeoceanographic and mantle circulation models.

By assembling the regional-scale tectonic reconstructions developed at the University of Lausanne (UNIL) during the last 20 years (Stampfli *et al.*, 1991, 1998, 2001, 2002a, 2002b, 2003, 2011, 2013; Stampfli, 1993, 2000; Stampfli and Pillevuit, 1993; Stampfli and Borel, 2002, 2004; Stampfli and Kozur, 2006; von Raumer *et al.*, 2006, 2009; Bagheri and Stampfli, 2008; Ferrari *et al.*, 2008; Moix *et al.*, 2008; von Raumer and Stampfli, 2008; Flores-Reyes, 2009; Stampfli and Hochard, 2009; Wilhem, 2010; Vérard *et al.*, 2012a; Vérard and Stampfli, 2013a, 2013b; von Raumer *et al.*, 2013), we have created a global plate tectonic model covering the whole Earth′s surface (*i.e.*, continental and oceanic realms) over the Phanerozoic Eon. Initially presented in Stampfli and Borel (2002) and

* Corresponding author. E-mail: Xian_verard@hotmail.com.
Received: 2014−09−17 Accepted: 2014−12−22

Stampfli and Borel (2004), the "dynamic plate boundaries" method then used to develop the model has been updated in the light of new studies and techniques.

The model presented herein corresponds to the model developed at UNIL, and purchased by Neftex Petroleum Consultant Ltd. in January 2010; it is therefore hereafter referred to as the UNIL model (v.2011, © Neftex). It is beyond the scope of the present paper to discuss the validity of each field study interpretation and the reader is asked to refer to the aforementioned papers for all the details. We focus upon: (1) further detailing the method and techniques employed to develop the global plate tectonic reconstructions; (2) comparing a series of tectonic factors stemming from the model with various proxies thought to reflect variations in plate tectonics, namely: mean oceanic ages and plate velocities versus sea-level variations, tectonic activity versus CO_2 and markers of glaciation extent, and length of collision zones and $^{87}Sr/^{86}Sr$ (Sr-ratio) isotopic changes. The goal is twofold: (1) validating the robustness of the model and (2) better comprehending the relationship between tectonics and such palaeoclimatic indicators. Using an innovative way to convert 2D maps into 3D topographic surfaces, the robustness of the model is tested more directly against sea-level and Sr-ratio variations in another paper (Vérard *et al.*, 2015).

2 Method —— From geodynamic units to tectonic plates

To reconstruct the Earth's history, we developed an approach in which the elementary units are named geodynamic units (GDUs; see definition below). Using geological data of geodynamic interest (*i.e.*, providing insights on geodynamical environments such as rift zone, passive margin, active margin, collision zone, *etc.*), the geological histories of GDUs are correlated through space and time to define larger scale geodynamic scenarios. In turn, the regional geodynamic scenarios are correlated to generate global scale plate tectonic models.

In plate tectonic modeling, the lithosphere is divided into smaller entities usually named "terranes". However, the latter term was used long before the advent of plate tectonics (d'Aubuisson de Voisins, 1819; Dana, 1863; Schardt, 1893) and his fundamental meaning has been a matter of hot debate (*e.g.*, Sengör *et al.*, 1990; Howell, 1995; Le Grand, 2002). As stated by Howell *et al.* (1985), a terrane is frequently defined as "*a fault bounded package of rocks of regional extent*" but we do think that such acceptance is far too imprecise and often leads to confusion. To avoid misunderstandings and supersede the term "terrane", we introduce the term "Geodynamic Unit" (GDU). A GDU describes the present-day smallest continental/oceanic fragment that underwent the same geodynamic evolution since 600 Ma (starting age of the model). The Earth′s history is reconstructed by redistributing the GDUs through space and time. The GDUs position is controlled by palaeogeographic data (*e.g.*, palaeoclimatology, palaeobiogeography, palaeomagnetism; see below) associated with geological data of geodynamic interest. A GDU is a spatial object used to carry information from present to past and is thus only a geological marker. GDUs are defined in the present-day configuration and keep their initial shape through time. Consequently, geological bending, stretching or shortening is not corrected within a GDU, but tight (untight) fits are used not to underestimate crustal extension (shortening). A map of GDUs as defined in the UNIL model (v.2011, © Neftex) is shown in Figure 1.

Geodynamic scenarios are usually represented as 2D cross-sections of regional scale (see an example in Figure 2). They are designed to account for the geological history of each GDU involved, and to respect physical parameters known to govern plate tectonics. As generally agreed (*e.g.*, Forsyth and Uyeda, 1975; Zhong and Gurnis, 1995; Anderson, 2001; Conrad and Lithgow-Bertelloni, 2002; Stern, 2004; Schellart *et al.*, 2007), we do consider that forces acting on plate boundaries (*i.e.*, slab pull, slab roll-back and ridge push) are the primary drivers of plate tectonics. Any change in plate motion must then be related to evolution of the boundary conditions. We stress that plate boundaries are lithospheric discontinuities which cannot appear spontaneously by themselves. In the UNIL model (v.2011, © Neftex), new plate boundaries can be created in the following configurations:

In extension: (1) lithospheric plate under extension can undergo rifting in its continental part because of the rheological weakness of the middle crust (*e.g.*, Cloos, 1993). A present-day example of such configuration is the Red Sea opening; (2) due to slab roll-back, arcs are also zones of weakness where extension may occur. In this case, the former ridge ceases and jumps into the arc. The latter splits into an abandoned arc and a new active arc (*e.g.*, the Lau ridges/Tonga-Kermadec active arc or the Marianas).

In convergence: (1) subduction can initiate if a lithospheric discontinuity pre-exists such as ridge failure and transform fault failure (*e.g.*, McKenzie, 1977; Mueller and Phillips, 1991; Müller *et al.*, 1998; Baes *et al.*, 2011a); (2) subduction propagation and subduction reversal (*i.e.*, revival of subduction behind the accreted terrane after colli-

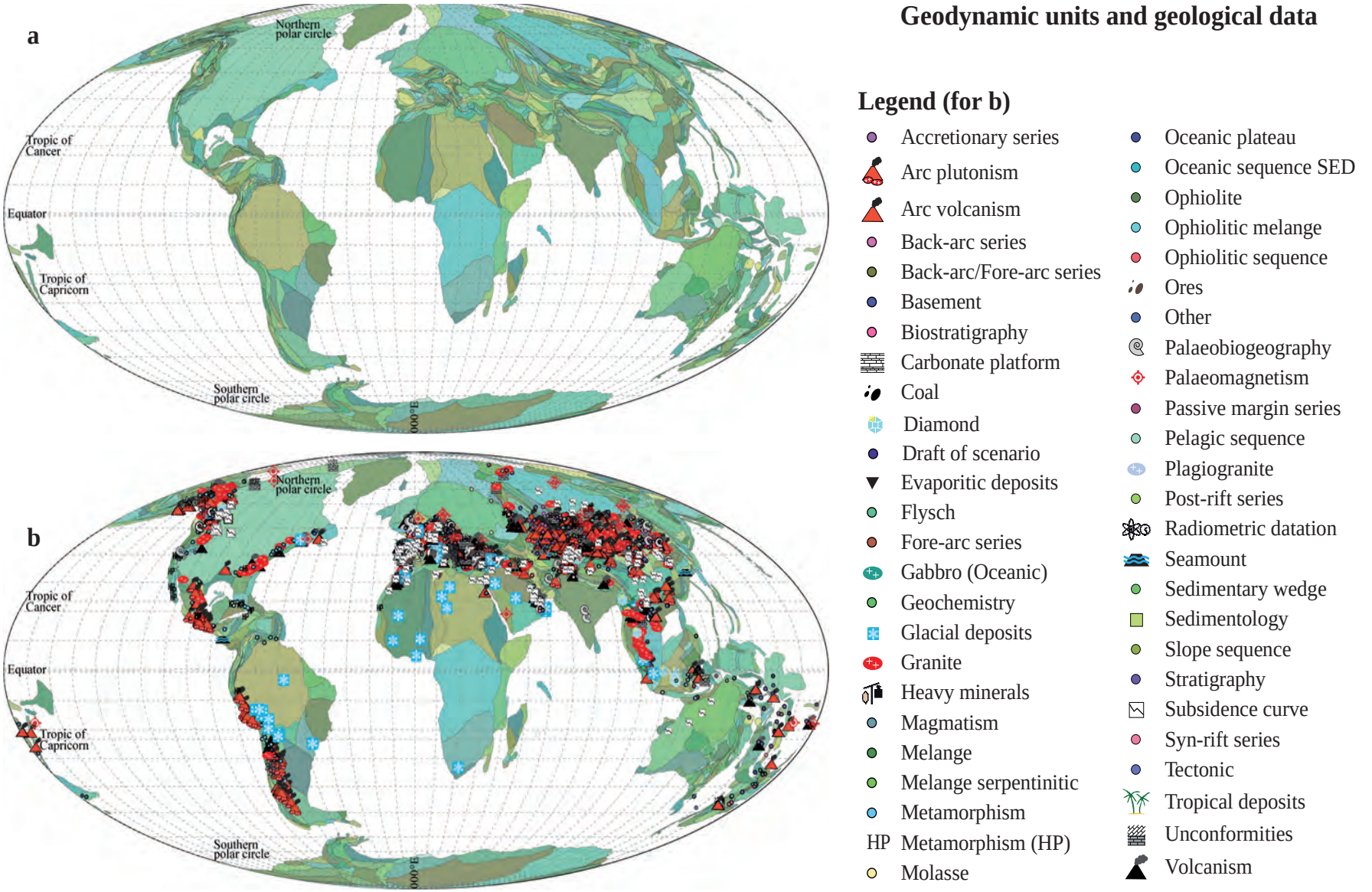

Figure 1 Geodynamic units and geological data of the UNIL model (v.2011; © Neftex). a−Geodynamic unit map of the world including 1046 entities (mainly continental, except in the Mediterranean, Caribbean and peri-Australian areas). Colors have been arbitrary attributed to each GDU to distinguish them one from the other, but have no meaning; b−Spatial distribution of 2897 among more data used in the model to constrain past reconstructions. The legend details the 50 possible types of geological data (see Hochard, 2008 for further discussion).

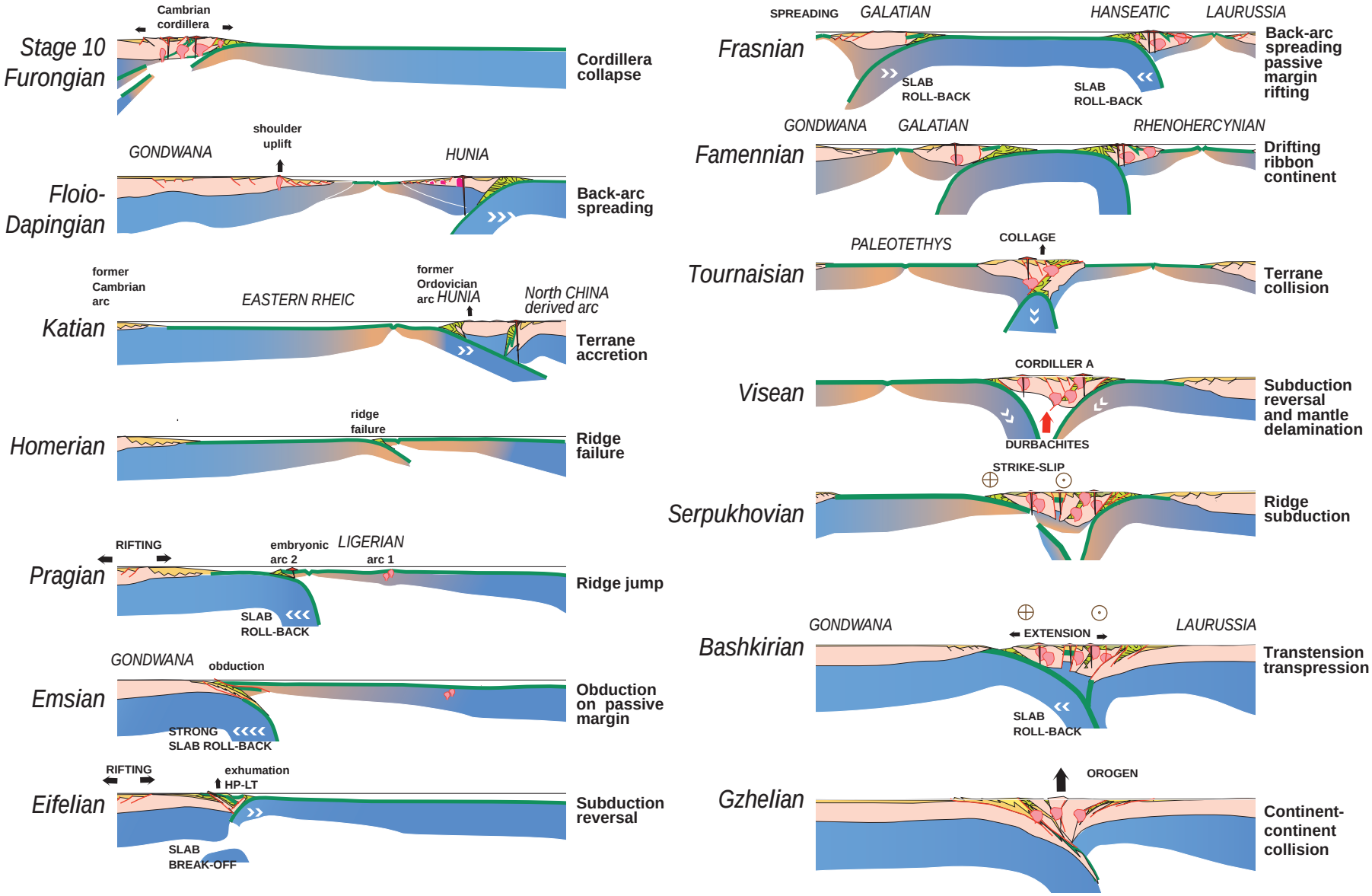

Figure 2 Example of geodynamic scenario after Stampfli *et al.* (2011; *op.cit.* Figure 2). Geodynamic scenarios are usually represented as cross sections. Here, a model of the evolution of the Gondwana margin from latest Cambrian (Stage 10; Furongian) to latest Carboniferous (Gzhelian; Upper Pennsylvanian). The sections are tied to Gondwana (left), so the continent to the right is changing through times. For the left part of the figure North China elements are facing Gondwana, whereas for the right side of the figure it is Laurussia. The horizontal scale is not respected.

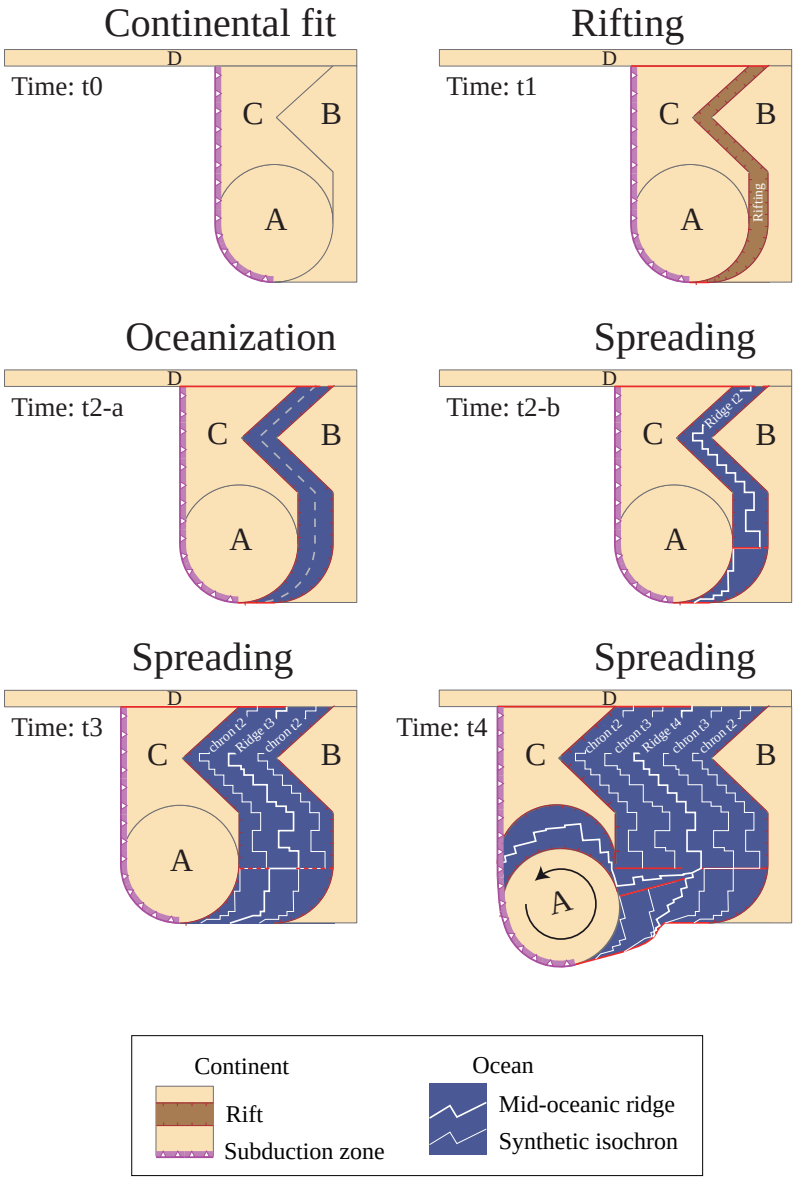

Figure 3 Technique used for the reconstructions, with in particular, definition of synthetic ridge and isochrons in disappeared oceans. See details in text.

sion in forward or reverse direction respectively) together with step faults (Baes *et al.*, 2011b) are the only processes that can turn a passive margin into an active margin. Continued aging of a passive margin alone, in particular, does not result in conditions favorable for transformation into an active margin (Cloetingh *et al.*, 1982, 1984).

To avoid unrealistic velocities, we arbitrarily limit plate velocity to a maximum of 22 cm·yr^{-1}. This value corresponds to the present-day highest equatorial plate velocity on Earth after DeMets *et al.* (1994). This value is of course subject to caution and was more used as warning sign during reconstruction; however, we did not need to strictly use this parameter to constrain the model.

A lot of reconstruction models are actually not constructed using plate tectonic principles but with an approach akin to continental drift. They use continental blocks (*i.e.*, similar to our GDUs) as individual entities moving their own way without paying enough attention to the plate in which the blocks are included. Although they have disappeared, past plate boundaries can be retrieved thanks to geological data. In the UNIL model (v.2011, © Neftex), a tectonic plate is an assemblage of GDUs fully surrounded by plate boundaries forming an interconnected network. Except in plate boundary areas, a tectonic plate is considered as an undeformable rigid body. No feature constituting a plate (in particular no GDU) can move its own way. This approach offers a strong control on plate motion since any data of a GDU belonging to a given plate

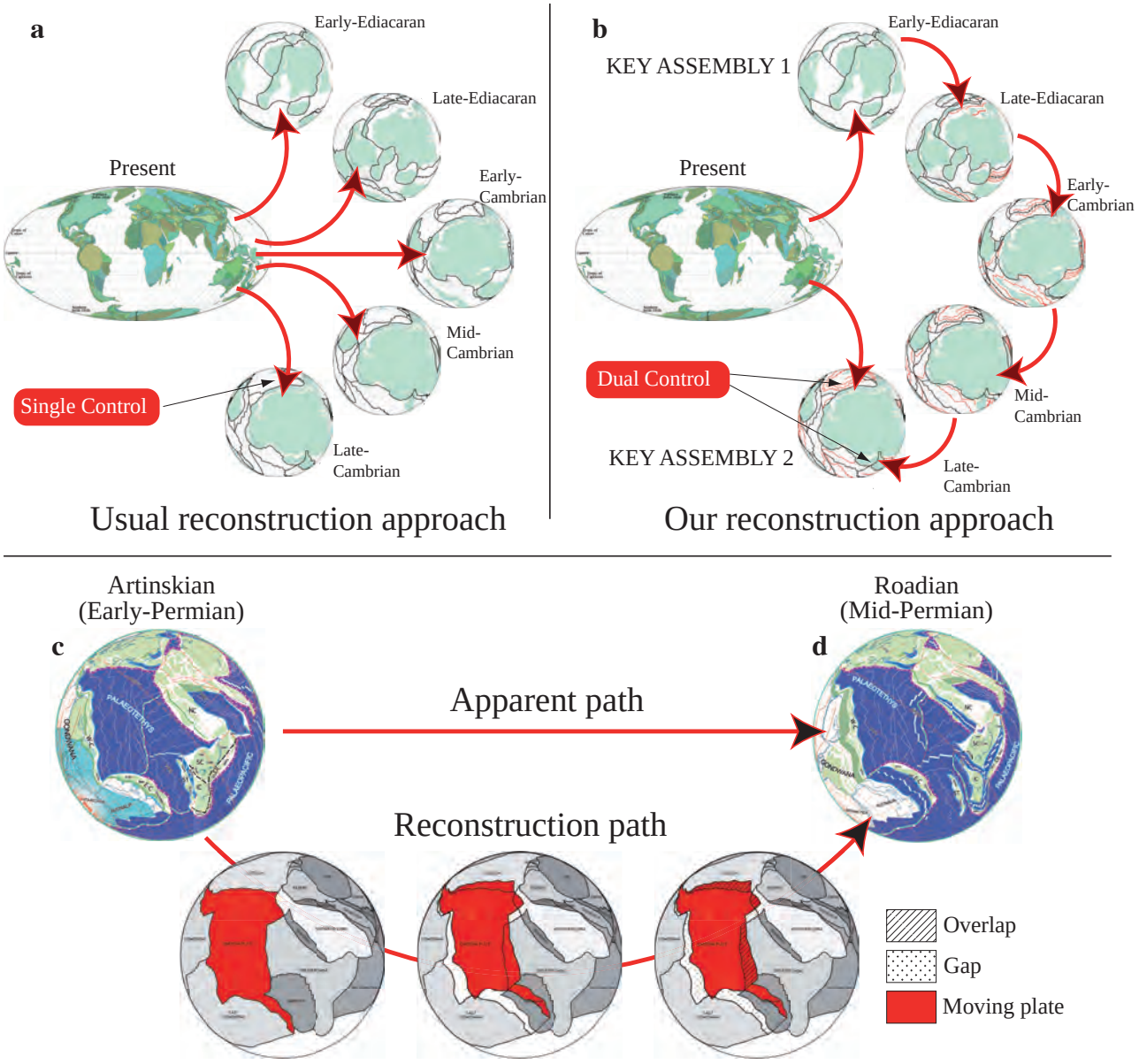

Figure 4 Comparison between the usual reconstruction approach and our approach. a−In the usual approach, the present-day continents are divided into blocks redistributed using palaeomagnetic data and palaeobiogeographic data available for each age; b−In our approach, the continental blocks (GDUs) are redistributed to form key assemblies (for which palaeomagnetic and palaeobiogeographic data are known and reliable) but the in-between time frames are reconstructed following geodynamic scenarios based on other geological data. Key assemblies are thus controlled twice. The coherence of the geological history is as important (if not more) as the raw data which often suffer large uncertainties; c and d−Detailed steps between two reconstructions. Plate positions are interpolated to go from c to d. As the plate polygons are preserved, overlaps and gaps can be identified which lead to the definition of new converging (*i.e.*, subduction or collision zones) or diverging (*i.e.*, ridges and rifts) plate boundaries. Reconstructions from Atinskian (mid-Cisuralian; Early Permian) to Roadian (early-Guadalupian; Middle Permian) after Ferrari *et al.* (2008). This figure is in part derivative from the Neftex Geodynamic Earth Model, © Neftex Petroleum Consultants Ltd., 2011.

helps to define the location of the entire plate. The motion of plates is controlled by the geodynamic scenarios. Knowing the positions of the GDUs and the timing of major geodynamic events (*e.g.*, continental break-up, collision, subduction initiation or reversal, *etc.*), one can trace the motion of plates.

For mid-oceanic ridges, for instance, the location and geometry are inferred from the global isochrons dataset of Müller *et al.* (2008a) where possible. For disappeared oceans, the exact shape of mid-oceanic ridges is not known, and will never be. However, during the continental break-up, if plate velocities and geometries are known, the

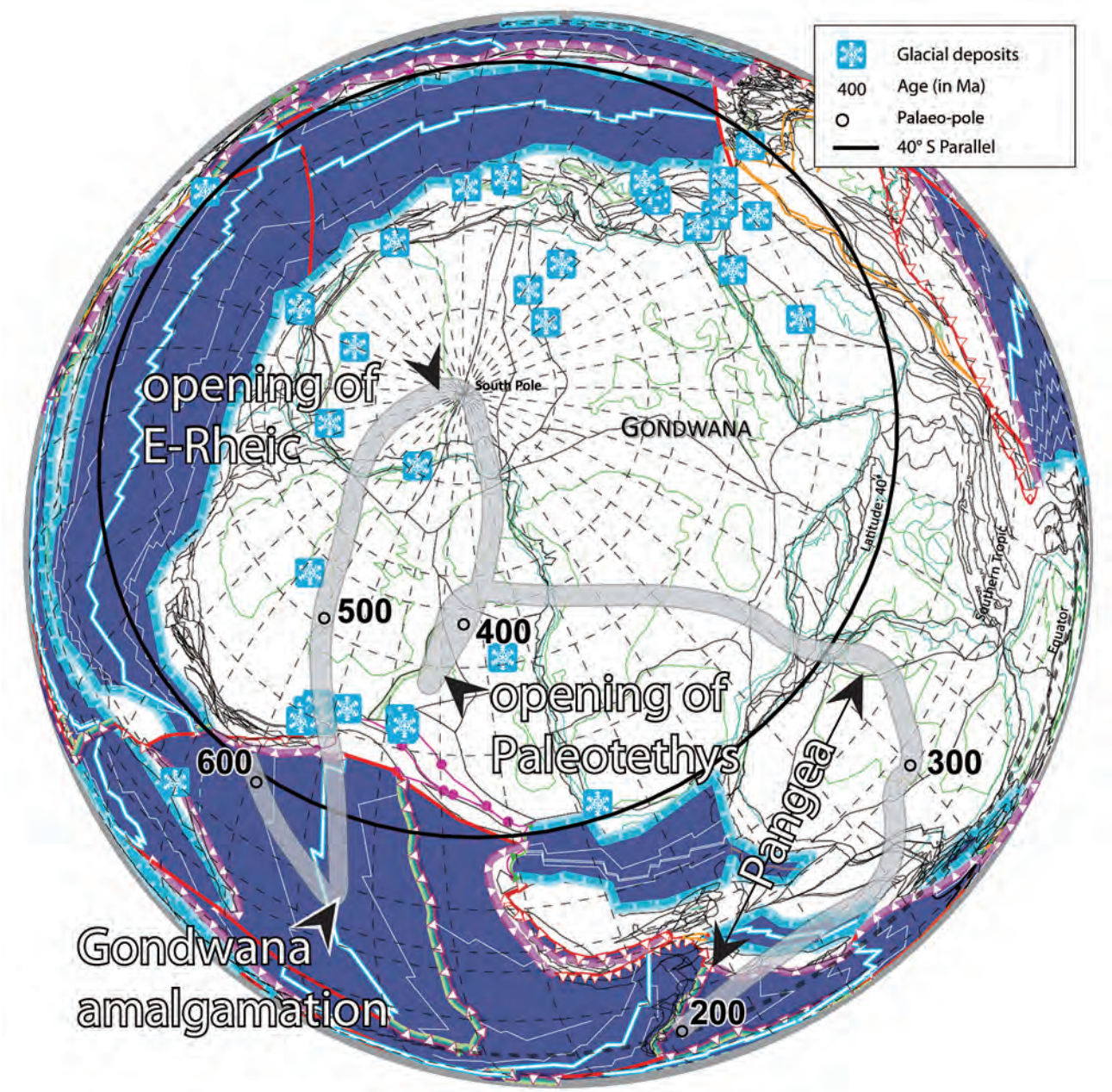

Figure 5 Apparent polar wander path for Gondwana after Stampfli *et al.* (2013; *op.cit.* Figure 5). 300 Ma to present-day palaeo-poles are from Torsvik and van der Voo (2002); Frasnian (early Late Devonian) to 300 Ma palaeo-poles are from Torsvik and van der Voo (2002). Older segments of the path are based on two key poles (at *ca.* 550 Ma and *ca.* 480 Ma) consistent in the studies of Schmidt *et al.* (1990), Bachtadse and Briden (1991), Li and Powell (2001), Torsvik and van der Voo (2002) and McElhinny *et al.* (2003). In the intervals, following the same approach as in Scotese and Barrett (1990), the pole locations are constrained using the global distributions of carbonates and glacial deposits. The present figure shows an example for Hirnantian time. Additionally we minimized the resulting velocity of Gondwana to keep a value near 8 cm·yr^{-1} comparable with its velocity between 300 Ma and 0 Ma. This figure is in part derivative from the Neftex Geodynamic Earth Model, © Neftex Petroleum Consultants Ltd., 2011.

space between the detaching and the left-over fragments (into which the new ridge formed) is constrained. As an example, Figure 3 shows how a continental block composed of two GDUs (A and B) is detached from GDU C at time t1. According to the geodynamic scenario established for these GDUs, the timing of the oceanization (in the sense of the presence of oceanic crust and/or denudated mantle) and the velocity are known (Figure 3; time t2-a). In the available space, a new ridge is designed (Figure 3; time t2-b) with transform segments following small circles of the rotation. From time t2 to time t3, the ridge becomes two symmetric synthetic isochrons, which strongly con-

strain the position of the next ridge. At time t4, the rotation of GDU A is then constrained by the plate geometry, in particular by the space for the triple junction to develop and by the spreading rate on the other side of the mid-oceanic ridge formed between A and C. By preserving the synthetic isochrons step after step, the uncertainties are reduced and the oceans are reconstructed.

The reconstruction work is carried out from past to present. Starting hitherto with a continental assemblage at 600 Ma, crustal material is added/removed in divergent/convergent areas marked by newly defined plate boundaries. From one reconstruction to the next, plate positions are interpolated and former plate polygons are first preserved to identify the diverging (gaps) and converging (overlaps) areas (Figure 4c and 4d). As for mid-oceanic ridges, new plate boundaries (*i.e.*, subduction zones, collision zones or transform faults) are defined in those restricted areas, limiting the uncertainties and ensuring the continuity in the model.

This approach is based on the relative movements of plates constrained by the GDUs. For major continental blocks (*i.e.*, Baltica, Laurentia, Siberia and Gondwana), published apparent polar wander paths (Torsvik *et al.*, 1996, 2008; Torsvik and van der Voo, 2002; Torsvik and Cocks, 2005; Cocks and Torsvik, 2007) were used and sometimes modified to fit palaeogeographic data and/or limit the velocity of the reference plate (see Figure 5 and Hochard, 2008 for further details). However, palaeo-poles are not sufficient as (1) they give no constraint in palaeolongitude (except in Torsvik *et al.*, 2008); (2) they are often subject to large uncertainties; (3) most of the time, they do not exist for smaller GDUs. To overcome this issue, we employed the trial-and-error method and performed numerous iterations. Like Scotese *et al.* (1999), we followed palaeogeographic principles and try to distribute GDUs thanks to rock deposits providing palaeoclimatic indications (*e.g.*, carbonates, evaporates, limestones, coals, tillites, *etc.*). Following Cocks and Torsvik (2002) for instance, we additionally use palaeo-faunas. But rather than trying to locate a continental block on the basis of a single study at all ages, we select key ages where palaeomagnetic, palaeoclimatic and palaeobiogeographic data are in good agreement for many blocks and define "key assemblies" (Figure 4b). In between frames are reconstructed following geodynamic scenarios. Supplementing the palaeomagnetic, palaeoclimatic and palaeobiogeographic data with a geodynamically consistent history offers an additional constraint ("dual control" in Figure 4b) which, in our opinion, represents a major step forward.

3 Geodynamic model and derivative maps

The UNIL model (v.2011, © Neftex) comprises 48 reconstructions extending back to 600 Ma every 5 Ma to 20 Ma (Figure 6a). On average, a reconstruction is made up of about 1700 features (lines, points, polygons under ArcGIS®) of 26 possible types describing the geodynamic context (*e.g.*, collision zone, mid-oceanic ridge, passive margin) or the palaeogeography (*e.g.*, basin limit, geographical marker) (see legend in Figure 9a). The model is based on 1046 GDUs associated with 2897 geological data distributed throughout the Phanerozoic (Figure 1 and temporal distribution in Figure 6b). A reconstruction is constrained on average by 267.4 geological data of 50 possible types (see legend in Figure 1 and Hochard, 2008 for further discussion) with a minimum of 86 data points at 6 Ma and a maximum of 481 data points at 330 Ma. At 600 Ma (first reconstruction), 83% of the Earth surface is reconstructed. This value rises gradually to reach 100% as early as 461 Ma (black squares in Figure 6a). The first reconstruction includes 509 GDUs only. However, once a GDU is present (*i.e.*, comes into existence) on a reconstruction, it is preserved and evolves to end up in its final present-day position. Consequently, the amount of GDU rises progressively according to the geological history (black line in Figure 6a). The smallest GDU is 0.183×10^3 km^2 large, and the largest is 1.65×10^7 km^2 large (Figure 7). For comparison, the widespread Earthbyte Plate Model 2009 (online data: http://www.earthbyte.org/Resources/earthbyte_plate_model_2009.html; Müller *et al.*, 2008a), which covers Mesozoic−Cenozoic time, includes much fewer blocks (195 blocks, ranging from 8.19×10^3 km^2 to 2.60×10^7 km^2 in size). We note that, in the model of Domeier and Torsvik (2014) extending back to 410 Ma, the number of blocks comes to 972.

In terms of tectonic plates, we note the linear relationship in logarithmic scale (with equation $Y = -1.809647848 \times X + 2.998827829$) suggesting a fractal behavior throughout the Phanerozoic (Figure 8). The motions of tectonic plates have been analyzed by Vérard *et al.* (2012b), with implications on rotational (tidal?) effects of the Earth.

The present model has been developed with ArcGIS® software. As all features making up the model are fully attributed (*e.g.*, type, age), one can quantify various tectonic parameters anywhere on the globe and of any geological time, and thereafter develop a series of derivative maps (Figure 9b−9d). Using measured and synthetic isochrons,

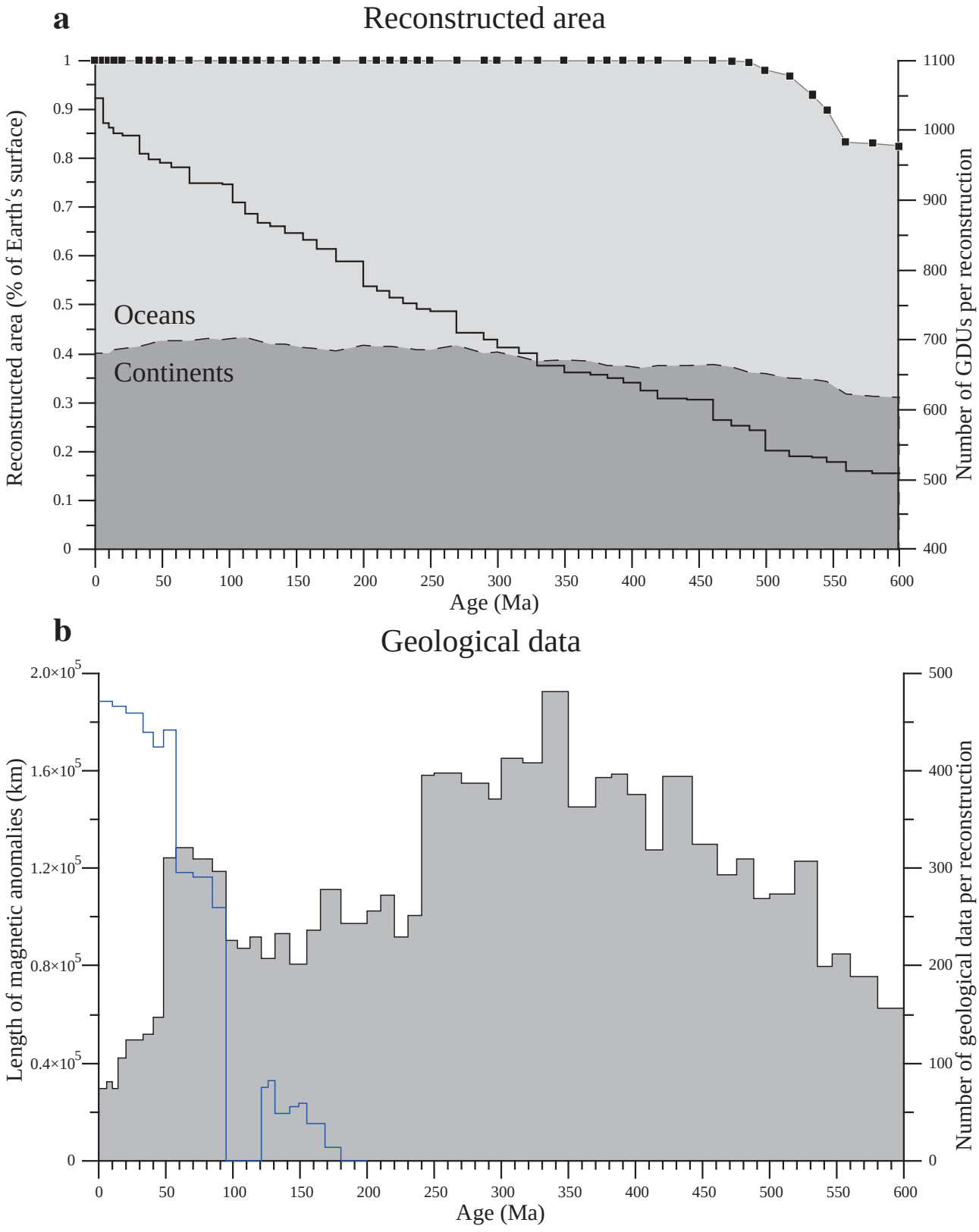

Figure 6 a−Evolution of the reconstructed area through time. Black squares represent the 48 reconstructions. Dashed line marks the limit between continental and oceanic area on each reconstruction. Black line represents the number of GDUs per reconstruction; b−Number of geological data used for each reconstruction. The minimum value is 74 (0 Ma), the maximum is 481 (330 Ma) and the average value is 267.4±101.0 (1σ) data per reconstruction. Blue line represents the length of measured isochrones available for each reconstruction after Müller *et al.* (2008a).

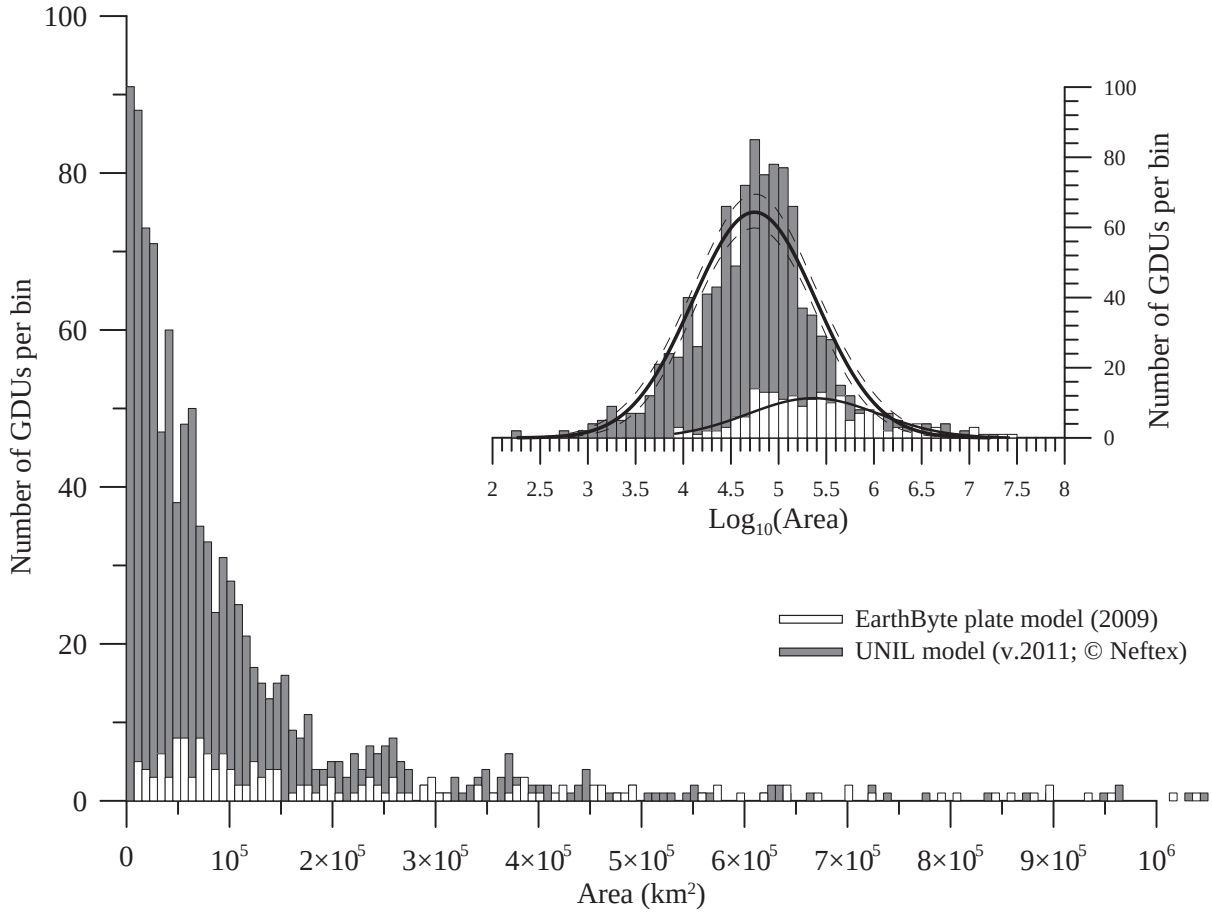

Figure 7 GDU size distribution. Number of GDUs per bins of 7500 km². The minimum size is 0.183×10^3 km² large and the maximum is 1.65×10^7 km² large. The distribution is logarithmically Gaussian and the mean value in log is of 4.74±0.65 corresponding to an area of 5.578×10^5 km². The EarthByte plate model (2009; http://www.earthbyte.org/Resources/earthbyte_plate_model_2009.html) is shown for comparison. The number of blocks in their model (equivalent to our GDUs) is much inferior, and their mean size is much larger (2.334×10^6 km²).

for example, we have computed palaeo-age maps representing the age of the oceanic crust relative to the age of the reconstruction (see Figure 9b). Using Euler rotation poles describing plate motions, we calculate the velocities and the convergence and divergence rates (Figure 9c; see also Vérard *et al.*, 2012b). Moreover, following the approach of Turcotte and Schubert (2002), we are able to convert palaeo-ages into lithospheric thicknesses in order to estimate the volume of subducted materials (Figure 9d).

4 Discussion —— Plate tectonic model and comparison with palaeoclimatic indicators

The model presented herein is based on years of field geology and thousands of literature studies. The output results are not strictly reproducible as input data are subjected to a degree of non-negligible interpretation. We do consider that temporal and spatial correlation of data reinforce their interpretation but one can always produce contradicting arguments that could deeply alter the model. Over the years, overhauls have occurred and some of our earliest publications are sometimes in contradiction with our latest version of the UNIL model (v.2011, © Neftex). Many issues integrated in the model are still a matter of sharp debate and inherent assumptions cannot be detailed herein. The publication of GDU rotation poles, in particular, would not be sufficient for other people to reproduce the model. Indeed, the redistribution of GDUs through space and time is only the first stage of the modeling process which must be followed by the redefinition of plate boundaries. Although strictly controlled by geological data, the latter step is in part subject to uncertainties and the ensuing result is proper to each author. Nevertheless, a first validation of our approach has been provided by the study of Hafkenscheid *et al.* (2006) which compared three

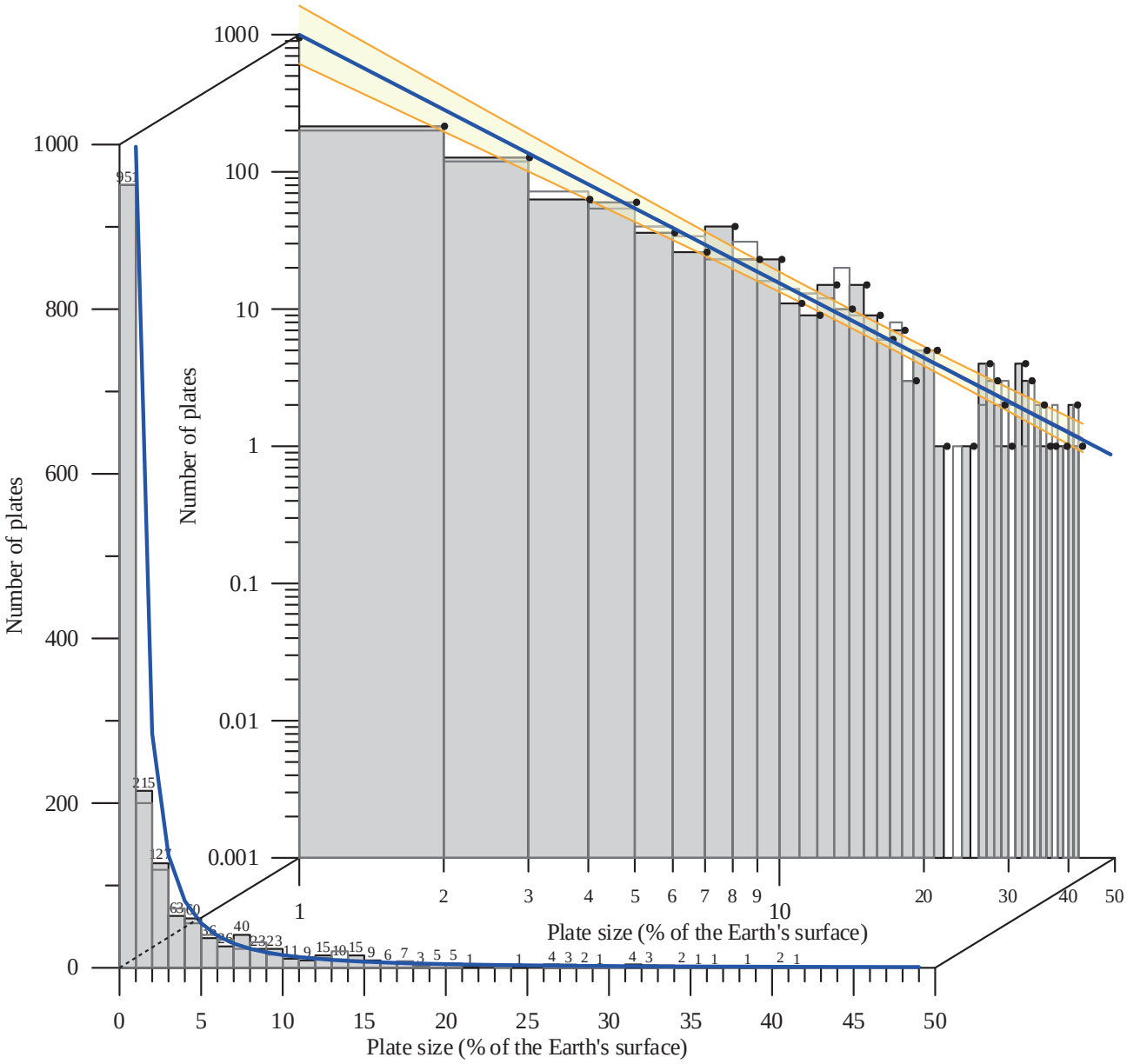

Figure 8 Plate size distribution throughout the Phanerozoic with linear scale in the foreground turned into log−log scale in the background. The linear relationship (blue) with its associated 95% confidence interval (orange) in log−log scale shows the fractal behavior of plate size.

tectonic models of Cenozoic−Mesozoic Tethyan evolution with mantle tomography and concluded, as did Webb (2012), that our solution was the most reliable.

Here, we opt for a different but complementary approach. We compare tectonic factors stemming from the reconstructions (2D maps on the globe) with separate parameters such as palaeoclimatic indicators known to be strongly linked with plate tectonics. We are aware that processes involved in climate are nonlinear and complex. They concern, all at once, the bio-, hydro-, litho- and atmosphere. They include positive and negative feedbacks which cannot be unveiled in a pure tectonic model. We, therefore, merely looked at first order (or large scale) correlations and did not expect to reproduce every single short scale variation.

4.1 Mean oceanic ages, plate velocities and sea-level variations

Using palaeo-age maps, we have calculated the average age of the oceanic crust at each reconstruction (Figure 10a). A noteworthy global negative trend can be observed. In the Early Cambrian (Fortunian), the oceanic crust is 16.8 million years old whereas, at present-day, the mean age is close to 65 million years old. The mathemati-

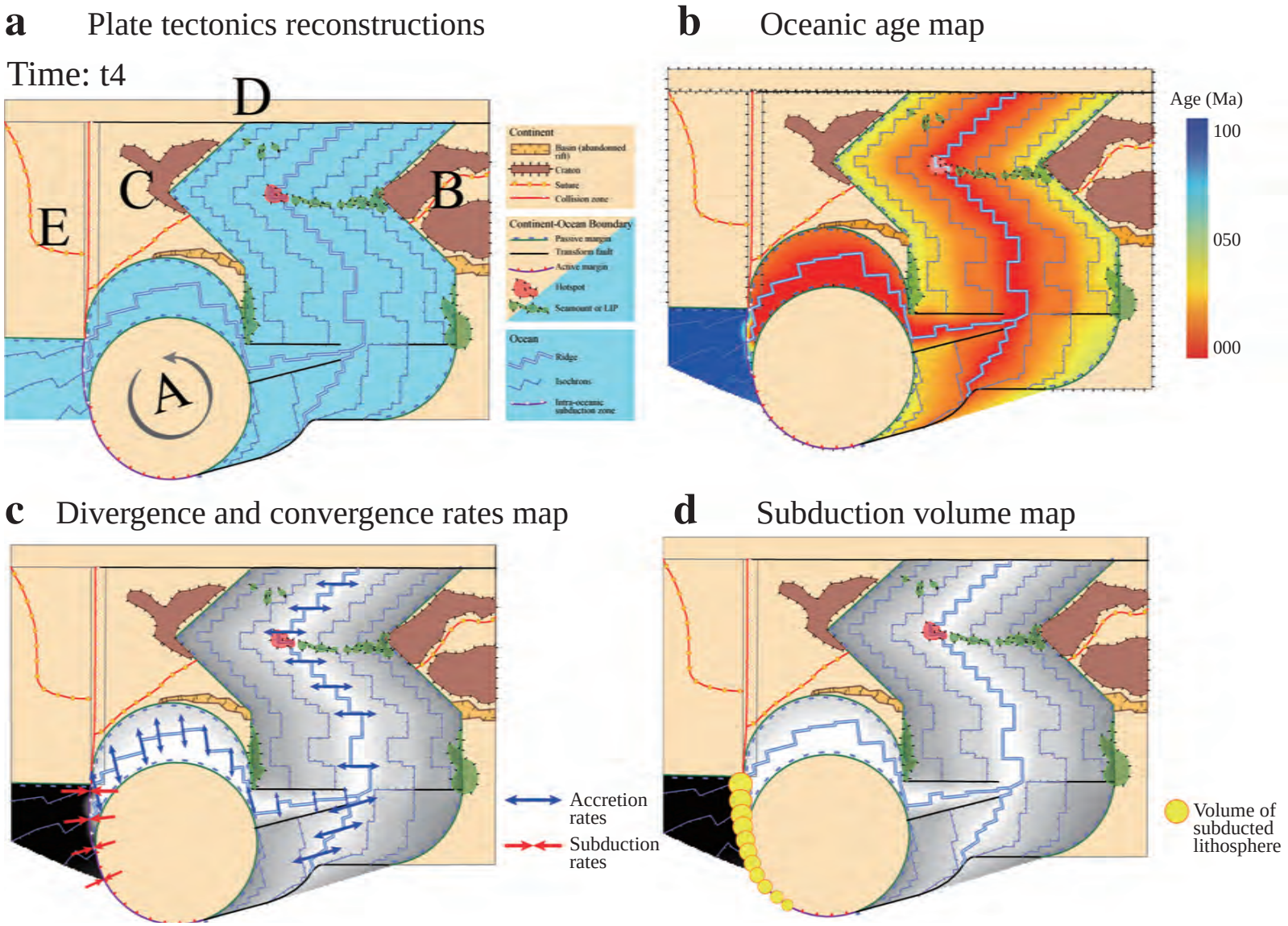

Figure 9 Example of schematic reconstructions and derivative maps. a−Reconstructions as per Figure 3. LIP = Large Igneous Province; b−Palaeo-age map stemming from the reconstructions. Ages are relative to the age of the reconstruction; c−Divergence (blue arrows) and convergence (red arrows) rates computed from Euler rotation poles along mid-oceanic ridges (accreted surface) and along trenches (consumed area) anywhere on the planet at any geological times; d−Using the approach of Turcotte and Schubert (2002), palaeo-ages are converted into lithospheric thicknesses to estimate the volume of subducted materials.

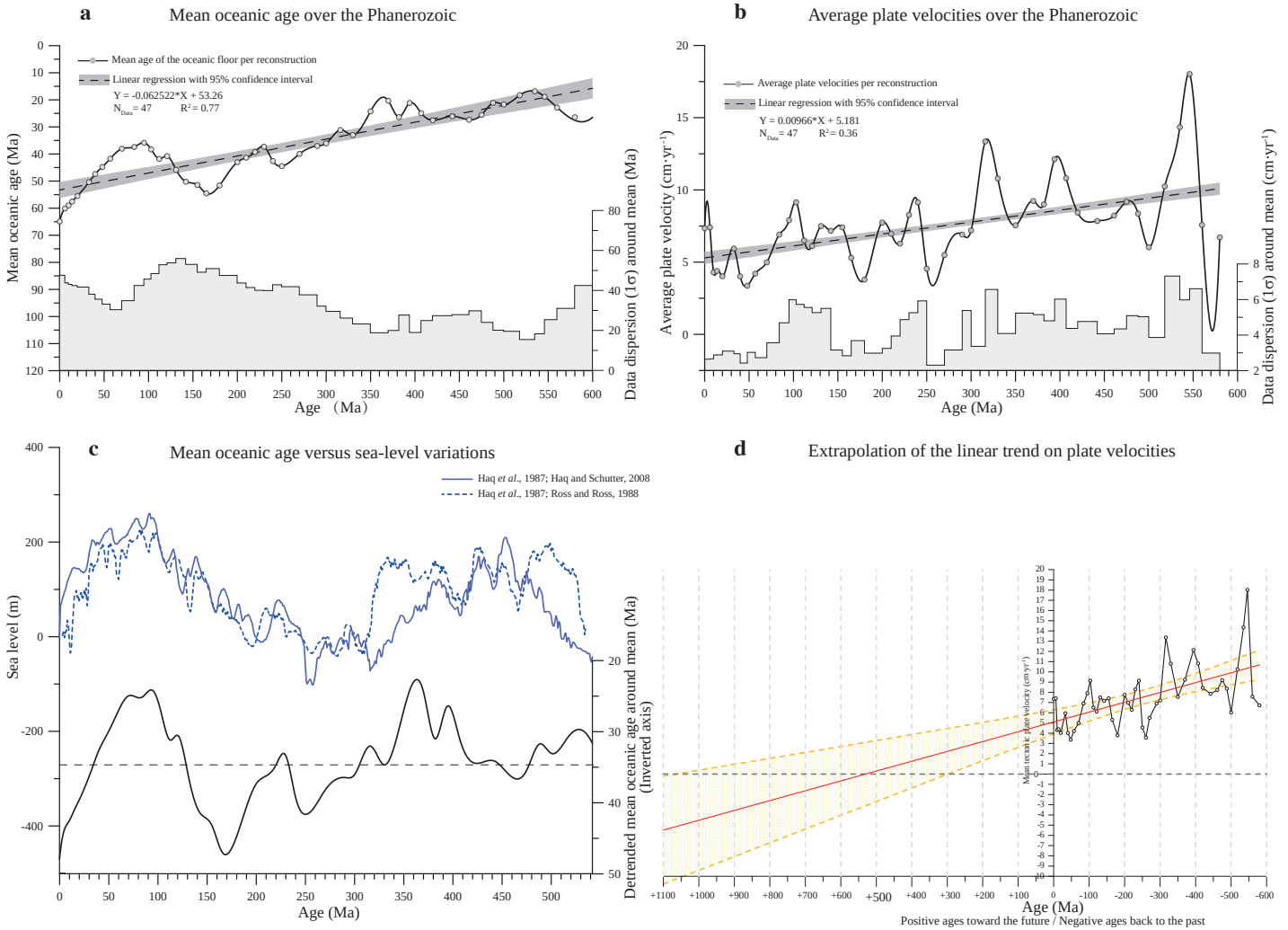

Figure 10 a−Mean palaeo-ages (*i.e.*, relative to the age of the reconstruction) of oceanic floor over the Phanerozoic; the corresponding linear trend is shown with its associated 95% confidence bounds. The grey step plot represents the standard deviation around the mean age at each reconstructed time slice and reflects the large dispersion around the mean value; b−Average velocities of plates for each reconstruction. Although the coefficient of determination is low ($R^2 = 0.36$), the overall decreasing trend is confirmed by the 95% confidence interval; c−Detrended oceanic mean age versus sea-level variations. Light blue, sea-level variations are from Haq *et al.* (1987) and Haq and Schutter (2008) (intermediate term); dark blue, sea-level variations are from Haq *et al.* (1987) and Ross and Ross (1988). The black curve represents the detrended mean oceanic ages around its mean value (34.65 Ma; this study); d−Extrapolation of the linear trend displayed in b, showing that mean tectonic plate velocity reaches zero cm·yr^{-1} (*i.e.*, stops) in *ca.* 500 Ma from now (dashed lines are 95% confidence limits) if the linear relationship is revealed to be true.

cal model (linear, logarithmic, *etc.*) behind this negative trend is unknown. However, a simple linear regression yields a secular decrease in mean oceanic age of −6.2% (coefficient of determination $R^2 = 0.77$, which is a classic statistical parameter). As the mean ocean ages, plate velocities (Figure 10b) also undergo a global decrease over the last 600 Ma (with a slope S equal to 0.0097 cm·yr^{-1}/Ma). Although the coefficient of determination is low ($R^2 = 0.36$), the overall decrease is statistically confirmed at the 95% confidence level. We infer that the global aging of the lithosphere due to the overall slowdown of the plates is related to the reduction of the tectonic activity. The latter is potentially due to the global cooling of the Earth which has long been recognized (*e.g.*, Kelvin, 1864; Turcotte, 1980; Labrosse and Jaupart, 2007) but never highlighted in a tectonic model. We note, furthermore, that when the linear trend (shown in Figure 10b) is extrapolated into the future, the line crosses the abscissa (*i.e.*, mean plate motion equals zero cm·yr^{-1}) at +500 Ma (and between +300 Ma and +1000 Ma at the 95% confidence level) suggesting the end of plate tectonics on Earth in this time frame (Figure 10d). Although one must be cautious with this because the decrease may well be nonlinear. One may think, therefore, that an evolution of Earth′s lithosphere similar to that of Mars might happen from then on.

Possible causes for global sea-level changes are multiple with various time-scales and amplitudes (see recent debate after the publication of Miller *et al.*, 2005). On a long-term time scale (10^7 yr to 10^8 yr), sea-level fluctuations result from changes in the volume of ocean basins which are significantly, if not primarily, controlled by variations of oceanic crust ages (*e.g.*, Hays and Pitman, 1973; Parsons and Sclater, 1977; Donovan and Jones, 1979; Parsons, 1982; Gaffin, 1987; Cogné *et al.*, 2006; Cogné and Humler, 2008; Müller *et al.*, 2008b). Eustatic sea-level reconstructions based on stratigraphic data have been carried out by various authors (*e.g.*, Vail *et al.*, 1977; Hallam, 1984; Haq *et al.*, 1987; Haq and Schutter, 2008). Although Hallam (1984) shows a strong negative trend (−360 m) over the last 600 Ma, Vail *et al.* (1977) suggests a weak negative trend, and Haq and Schutter (2008) gives a positive trend. A recent study by Parai and Mukhopadhyay (2012) further suggests that the global oceanic volume is near steady-state and that the observed trends are within the uncertainties. For comparison with the most recent study of Haq and Schutter (2008), we reduced the mean oceanic age from its secular trend (Figure 10c). At very first approximation, the resulting curve mimics the sea-level variation signal, especially for the last 450 Ma. Prior to 450 Ma, the mean age value is subject to caution as the reconstruction model does not cover the entire Earth surface. The possible absence of a global decreasing trend in the sea-level variation curve can be explained by the offsetting effect of plate deceleration. As the plates are moving slower, the spreading rates are decreasing (Figure 11a; grey line). As a response, due to changes in the volume and composition of melt and to chemical variations in basalt composition (Klein and Langmuir, 1987; Keen *et al.*, 1990; Bown and White, 1994; Humler *et al.*, 1999), the initial ridge depth rises inducing a global uplift of the whole oceanic basement (see also Kominz, 1984; Stein and Stein, 1992; Niu and Hekinian, 1997; Small and Danyushevsky, 2003; Vérard *et al.*, 2011, 2015). The main mismatch between the sea level and the mean oceanic age curves observed around 170 Ma might result from the same process. The drop in mean oceanic age may be counterbalanced by a coeval velocity drop (Figure 11b) and is thought to have, therefore, no visible impact on the sea-level curve.

The parallel between palaeo-ages and sea-level variations, even before 180 Ma, highlights the robustness of the reconstruction method for vanished oceans. The result is further confirmed by using a full topography (Vérard *et al.*, 2015). However, we emphasize that the average value given here (*i.e.*, the arithmetic mean) is not strictly statistically representative as the surface/age distribution is not necessarily Gaussian distributed. Moreover, if predominant, the mean age of the oceanic lithosphere is not the only driver of the eustatic sea-level change. Various processes, other than mid-oceanic ridge dynamics, can affect sea level over tens or hundreds of millions of years (*e.g.*, continental lithosphere variations, oceanic sediments volume changes, ocean temperature variations, ocean volume variations, *etc.*).

4.2 Tectonic activity, carbon dioxide and glaciation

When analyzing the relationship between the area of preserved oceanic lithosphere per unit time versus age, Parsons (1982) and later Rowley (2002) observed a linear decrease in the area of ocean age with increasing age. Such a linear trend is contrary to what one would expect if oceanic accretion rates varied significantly through time. As an explanation, the authors raised the hypothesis of a constant destruction (and therefore production) rate of the oceanic crust through time. However, a long term steady-state production rate is unlikely for, at least, three reasons: (1) the present-day spreading rates vary significantly from ocean to ocean (from 0.73 cm·yr^{-1} in the Arctic Ocean to 18 cm·yr^{-1} in the Pacific Ocean; DeMets *et al.*, 1990); (2)

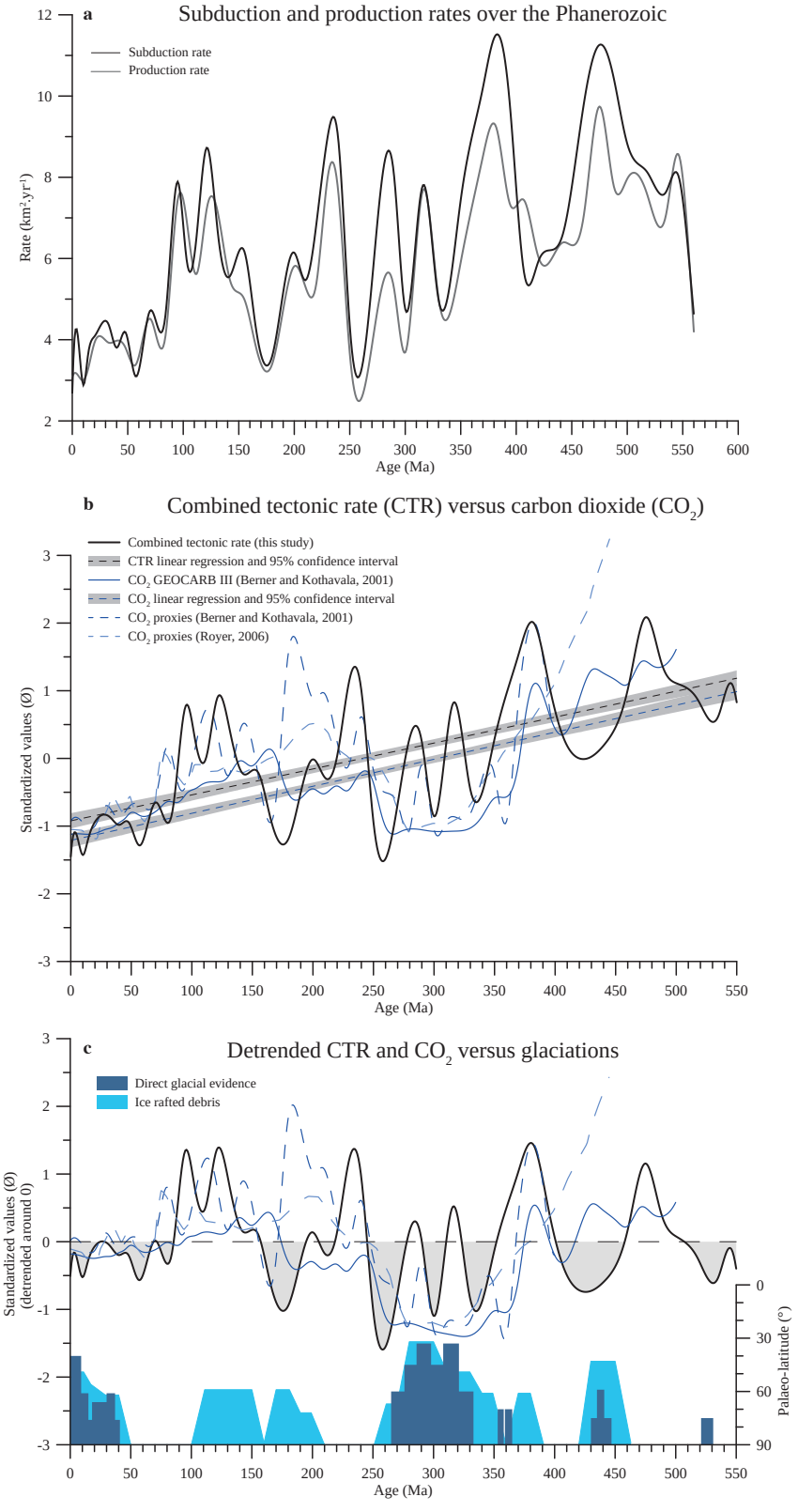

Figure 11 a−Evolution of subduction and production rates over the Phanerozoic. Subduction rates (black line) and production rates (grey line) are defined as the area of subducted/accreted material between two successive reconstructions; b−"Tectonic activity" (TA; black line) is the mean value between subduction and production rates. Linear decreasing trends of TA ($R^2 = 0.44$) and CO_2 ($R^2 = 0.49$) are confirmed by 95% confidence intervals. The slopes are very similar ($S_{TA} = 0.00394$ and $S_{CO2} = 0.00399$); c−Direct glacial evidence (tillites, striated bedrock, *etc.*; dark blue) are from Royer *et al.* (2004) modified after Crowley and Burke (1998). Ice rafted debris (light blue) are from Frakes and Francis (1988).

spreading rates calculated thanks to preserved magnetic anomalies have strongly varied since Jurassic times (Kominz, 1984; Larson, 1991; Müller *et al.*, 2008a). In Gaffin′s (1987) model, for instance, the production rates in the Cretaceous are almost double relative to present-day; (3) tectonic processes such as ridge jump, ridge subduction, back-arc opening, continental breakup and continental collision are frequent and result in abrupt changes in plate motions. Moreover, Demicco (2004) showed that it was possible to achieve the same linear relationship as in Parsons (1982), even accounting for non-steady-state production of oceanic crust with time. Figure 11a represents the subduction and production rates (in $km^2 \cdot yr^{-1}$) stemming from the UNIL model (v.2011, © Neftex; defined as the area of subducted/produced material divided by the length of trenches/ridges respectively). For the Cretaceous, the results are in good agreement with the studies of Gaffin (1987), Larson (1991), Müller *et al.* (2008b) on production rates and Engebretson *et al.* (1992) on subduction rates, but in contradiction with that of Cogné and Humler (2006), presenting slightly lower rates. Over the Phanerozoic, we can observe that production rates have strongly varied between a minimum of 2.48 $km^2 \cdot yr^{-1}$ and a maximum of 9.74 $km^2 \cdot yr^{-1}$ which is contradictory to the steady-state model.

Although, in Figure 11a, the production and subduction rates are closely related, the two curves present local discrepancies due to intra-plate deformations (*i.e.*, extension in rifting and shortening in collision zones). We thus introduce a "tectonic activity" (TA) parameter representing the average value between production and subduction rates and reflecting the global tectonic activity of the Earth. In order to compare parameters having different units, the values are standardized using the following equation (eq. 1):

$$Y_i = (X_i - \mu) / \sigma \qquad \text{(eq. 1)}$$

where, μ is the mean and σ is the standard deviation of the dataset.

Global plate motion changes have a predominant effect on long term variations of carbon dioxide (*e.g.*, Berner *et al.*, 1983; Lasaga *et al.*, 1985). During orogenies, the weathering of silicate rocks removes carbon from the atmosphere (by fixing it as additional carbonate; *e.g.*, Urey, 1952). The return of this carbon to the atmosphere via metamorphism, diagenesis and volcanism may take hundreds of millions of years. Such delay can result in an imbalance in CO_2 exchanges between atmosphere and rock reservoirs. Carbon dioxide variations are thus closely linked to the rate of sea-floor generation and subduction. We note that models developed to simulate the Phanerozoic evolution of atmospheric CO_2 composition (Berner and Kothavala, 2001; Wallmann, 2004; Berner, 2006) use weathering and degassing variations due to tectonics as key input parameters.

Our data are compared with the GEOCARB III CO_2 model of Berner and Kothavala (2001) associated with the proxy data of Berner and Kothavala (2001) and Royer (2006) based on palaeosols, stomata, phytoplankton, boron and liverworts analyses (Figure 11b). At the first order, the records have some good parallels. As expected (following palaeo-ages and plate velocities), the TA undergoes a global decrease over the Phanerozoic. The trend is indeed remarkably similar with the overall downward trend of the CO_2 curve (slopes are $S_{TA} = 0.00394$ and $S_{CO2} = 0.00399$), highlighting the link between CO_2 and tectonics. In details, short term fluctuations (10 Ma to 20 Ma) observed in the TA signal are rarely reflected in the GEOCARB III model whereas they are sometimes observed in the proxies. Albeit not statistically significant, the agreement is better on the larger scale. From the Cambrian to the Silurian (600 Ma to 400 Ma), high levels of CO_2 correspond to high levels of TA. In the same way, the CO_2 drop extending from the Early Devonian to the Early Permian (380−280 Ma) is coeval with a lowering of TA. Last, from 150 Ma to the present, the global decrease of the CO_2 coincides with a reduction of TA. The secular decreasing trend of CO_2 has long been recognized. An explanation is given by Berner (2004) who showed that the negative slope of the CO_2 curve is flattened when holding the solar luminosity constant over the time. Conversely, a slow increase in the luminosity of the sun causes warming, faster weathering and consequent CO_2 removal from the atmosphere to be fixed ultimately as carbonates. One of the major features noticeable both in the GEOCARB III model and in proxy estimates is the very low level of CO_2 observed during the Permo-Carboniferous. After Berner (1998), a primary reason for this drop was the rise of large vascular land plants, which accelerated weathering and led to the burial of large quantities of organic matter in sediments. Here, we can see that, coeval with the emergence of large vascular plants, a strong decrease of tectonic activity occurred. The two processes likely acted in the same direction.

Carbon dioxide is thought to be the primary impacting factor on climate (Royer *et al.*, 2004). Latitudinal extension of glaciation evidence (Frakes and Francis, 1988; Frakes *et al.*, 1992; and modified from Crowley and Burke, 1998 in Royer *et al.*, 2004) is thus compared with tectonic activity and CO_2 curves, detrended from their secular decrease (Figure 11c). The "tectonic activity" (TA) curve is

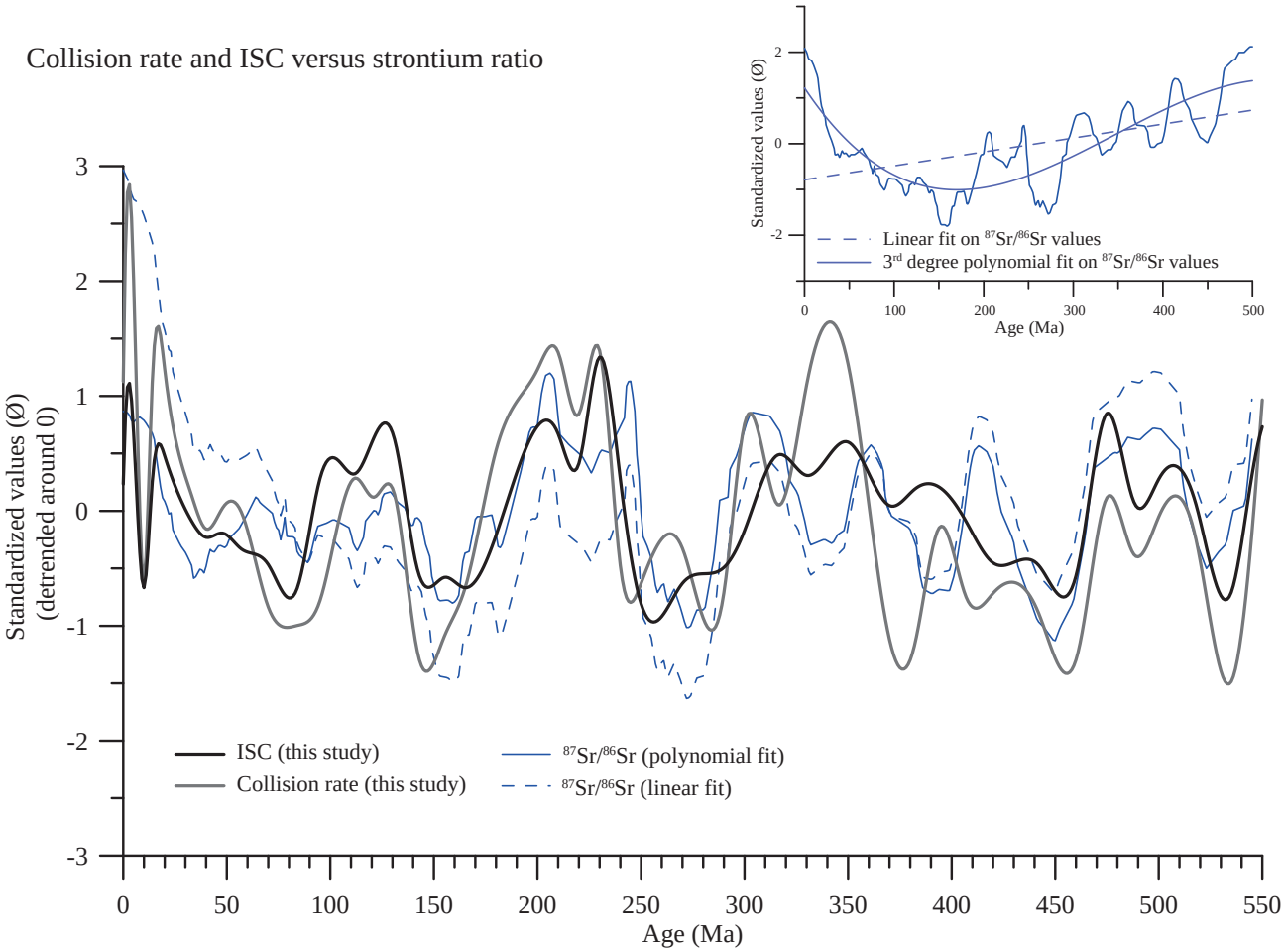

Figure 12 Comparison between reduced (or detrended) curves: "impact strontium curve" (ISC —— black line; see text), collision rates (grey line) and strontium ratio (blue lines). Inset: $^{87}Sr/^{86}Sr$ ratio after Prokoph *et al.* (2008) showing the two fits used for data reduction.

in good agreement with the glaciation records. Not only do the long-lived Paleozoic and Cenozoic glaciations show up as relatively negative values in the detrended TA curve (Figure 11c), but also the shorter and sometimes less firmly identified Early Cambrian (Crowley and Burke, 1998), Late Ordovician (*e.g.*, Saltzman and Young, 2005; Cherns and Wheeley, 2007) and Late Jurassic ones (*e.g.*, Dromart *et al.*, 2003; Suan *et al.*, 2010). Only the short-lived Late Devonian to Early Carboniferous glaciation (*e.g.*, Dickins, 1993) is not detectable with the model, which is visible in the CO_2 records. The existence of a relatively cool period between the Middle Jurassic and the Early Cretaceous, if it exists (Alley and Frakes, 2003), is neither supported by the CO_2 model and proxies nor by the tectonic model (UNIL model, v.2011, © Neftex).

4.3 Collision zones and strontium ratio

Strontium data are probably the most reliable isotopic record available for the whole Phanerozoic. Since no strontium isotopic fractionation occurs during carbonate precipitation and deposition, isotopic ratios measured from carbonates reflect that of seawater (Francois and Walker, 1992). The current strontium composition of seawater is a balance between inputs of high $^{87}Sr/^{86}Sr$ (*ca*. 0.715) due to the weathering of continental igneous rocks and low $^{87}Sr/^{86}Sr$ (*ca*. 0.703) resulting from fluid exchanges in seafloor hydrothermal systems. The 0.715 Sr-value for continental rocks is a weighted average between the presently exposed ^{87}Sr-enriched (*ca*. 0.718) old shields and ^{87}Sr-depleted (*ca*. 0.705) young igneous rocks, which is close to the oceanic Sr-ratio (*ca*. 0.709; Francois and Walker, 1992 and references therein). Therefore, the oceanic Sr-ratio can be presumed as a balance between the accretion of new oceanic crust and the exposure and weathering of old igneous rocks during collisions. In most box models developed to simulate the Phanerozoic seawater composition, the Sr-ratio of oceans is used as a proxy of mountain building (see *e.g.*, Berner, 1994, 2006; Wallmann, 2001).

For comparison purposes, we computed an "impact strontium curve" (ISC) (Figure 12) representing the average between the standardized values of production and collision rates. Note that, in the UNIL model (v.2011; © Neftex), a distinction is made between active collision zones (*i.e.*, converging plate boundaries) and suture zones (inactive collision zones located inside plates). The collision rate is defined as the overlapped area between two plates during a collision divided by the length of the collision zone. Although suture zones (*i.e.*, old and mostly inactive collision zones) also correspond to mountain belts, they are not taken into account in the ISC calculation (see Vérard *et al.*, 2015 for alternate calculation). Another bias could also stem from the lack of consideration of the rock age involved in the collision since young and old igneous rocks have opposite $^{87}Sr/^{86}Sr$ values. Last, ISC does not account for spatial distributions of collision zones and precipitations which might be of major concern (Tardy *et al.*, 1989). Newly created mountain belts, indeed, have no impact on $^{87}Sr/^{86}Sr$ ratio if they are not subject to erosion.

Using a comprehensive database of low-Mg calcitic fossil shells, Prokoph *et al.* (2008) demonstrated that among $^{87}Sr/^{86}Sr$, $\delta^{34}S$, $\delta^{18}O$ and $\delta^{13}C$ isotopes, the $\delta^{18}O$ record was the only record with a significant linear trend through the Phanerozoic. However, Veizer *et al.* (1999) established a strong correlation between the $^{87}Sr/^{86}Sr$ and the $\delta^{18}O$ signals which implies that strontium ratio should undergo a similar decrease over the Phanerozoic. As a consequence, in order to compare with the ISC, we have detrended the $^{87}Sr/^{86}Sr$ curve, once with a linear fit (with a poor R^2 value of 0.21) and once with a third degree polynomial fit (with a better R^2 value of 0.68). Whatever the method chosen, the UNIL model (v.2011, © Neftex) follows a good agreement with the detrended $^{87}Sr/^{86}Sr$ variations (Figure 12). Except during the Devonian−Carboniferous times, the ISC reproduces correctly most of the main Sr-ratio maxima and minima. Three causes may be invoked for the remaining local temporal shifts (particularly between 450 Ma and 350 Ma): (1) errors in the geodynamical model cannot be ruled out, and the model should therefore be revised if incorrect; (2) as the ISC results from a simple arithmetic mean, no consideration is given to the relative weights of old versus young igneous rocks and hydrothermal flux versus weathering flux; (3) the lack of temporal integration in the calculation of instantaneous production and collision rates. However, even if the ISC calculation seems relatively crude in comparison to the complexity of the strontium cycle, the correlation between the two curves is better than when one only considers the collision rates (grey curve on Figure 12). This underlines again the robustness of the reconstruction approach for vanished oceans.

5 Conclusions

We have developed the first global and physically coherent geodynamic model covering the entire Earth's surface for the whole Phanerozoic. For the first time, (1) a long term decrease of plate velocities (together with an aging of the oceanic crust, as expected) is observed in a set of global reconstructions; (2) we have been able to quantify oceanic production rates over the past 600 Ma and the results support the idea of a non-steady-state production of oceanic crust with time. We speculate that the overall decrease of tectonic activity is a consequence of global cooling of the Earth system.

In their study, Veizer *et al.* (1999) established a strong correlation between $^{87}Sr/^{86}Sr$, $\delta^{18}O$ and $\delta^{13}C$ variations over the Phanerozoic at any resolution greater than 1 Ma. Without further evidence, the authors state that this correlation suggests that the exogenic system (defined as litho-, hydro-, atmo-, and biosphere) was strongly driven by tectonic forces. All calculations shown herein are based on 2D spherical maps. More direct comparison of sea-level changes and strontium fluctuations is studied using an innovative 3D conversion (full topography) of the present model (Vérard *et al.*, 2015). Nevertheless, the first order correlation between the tectonic factors (*i.e.*, plate velocities, mean oceanic ages, accretion, subduction and collision rates) stemming from the UNIL model (v.2011; © Neftex) with a combination of palaeoclimatic indicators (*i.e.*, Sr-ratio, atmospheric carbon dioxide, sea-level variations and glacial deposits) supports the idea that plate tectonics has a predominant effect on climate at a scale of 10^7 yr^{-1} to 10^8 yr^{-1}.

Acknowledgements

We gratefully thank all members of the Prof. Stampfli's working group for sharing their data, ideas, and time with us. The Institute of Geology and Palaeontology of the University of Lausanne (UNIL) and the Swiss National Fund (SNF) are equally acknowledged for funding the present work. We thank Dr. Karin Warners-Ruckstuhl and Dr. Xiu-Mian Hu, for their comments and suggestions. The geodynamic model is now the property of Neftex Petroleum Consultants Ltd., with license to UNIL. We gratefully acknowledge the permission from Neftex Petroleum

Consultants Ltd. to publish these results.

References

Alley, N. F., Frakes, L. A., 2003. First known Cretaceous glaciation: Livingston Tillite Member of the Cadna-owie Formation, South Australia. Australian Journal of Earth Sciences, 50: 139−144.

Anderson, D. L., 2001. Top-Down Tectonics? Science, 293: 2016−2018.

Bachtadse, V., Briden, J., 1991. Palaeomagnetic constraints on the position of Gondwana during Ordovician to Devonian times. In: McKerrow, W. S., Scotese, C. R., (eds). Paleozoic Palaeogeography and Biogeography. Geological Society Memoir, 43−48.

Baes, M., Govers, R., Wortel, R., 2011a. Subduction initiation along the inherited weakness zone at the edge of a slab: Insights from numerical models. Geophysical Journal International, 184: 991−1008.

Baes, M., Govers, R., Wortel, R., 2011b. Switching between alternative responses of the lithosphere to continental collision. Geophysical Journal International, 187: 1151−1174.

Bagheri, S., Stampfli, G. M., 2008. The Anarak, Jandaq and Posht-e−Badam metamorphic complexes in central Iran: New geological data, relationships and tectonic implications. Tectonophysics, 451: 123−155.

Berner, R. A., 1994. GEOCARB II: A revised model of atmospheric CO_2 over Phanerozoic time. American Journal of Science, 294: 56−91.

Berner, R. A., 1998. The carbon cycle and carbon dioxide over Phanerozoic time: The role of land plants. Philosophical Transactions of the Royal Society of London. Series B: Biological Sciences, 353, 1365: 75−82.

Berner, R. A., 2004. The Phanerozoic Carbon Cycle: CO_2 and O_2. New York: Oxford University Press, 159.

Berner, R. A., 2006. GEOCARBSULF: A combined model for Phanerozoic atmospheric O_2 and CO_2. Geochimica et Cosmochimica Acta, 70: 5653−5664.

Berner, R. A., Kothavala, Z., 2001. GEOCARB III: A revised model of atmospheric CO_2 over Phanerozoic time. American Journal of Science, 301: 182−204.

Berner, R. A., Lasaga, A. C., Garrels, R. M., 1983. Carbonate-silicate geochemical cycle and its effect on atmospheric carbon dioxide over the past 100 million years. American Journal of Science, 283: 641−683.

Bown, J. W., White, R. S., 1994. Variation with spreading rate of oceanic crustal thickness and geochemistry. Earth and Planetary Science Letters, 121: 435−449.

Cherns, L., Wheeley, J. R., 2007. A pre-Hirnantian (Late Ordovician) interval of global cooling —— The Boda event re-assessed. Palaeogeography, Palaeoclimatology, Palaeoecology, 251: 449−460.

Cloetingh, S. A. P. L., Wortel, M. J. R., Vlaar, N. J., 1982. Evolution of passive continental margins and initiation of subduction zones. Nature, 297: 139−142.

Cloetingh, S. A. P. L., Wortel, M. J. R., Vlaar, N. J., 1984. Passive margin evolution, initiation of subduction and the Wilson cycle. Tectonophysics, 109: 147−163.

Cloos, M., 1993. Lithospheric buoyancy and collisional orogenesis: Subduction of oceanic plateaus, continental margins, island arcs, spreading ridges, and seamounts. GSA Bulletin, 105: 715−737.

Cocks, L. R. M., Torsvik, T. H., 2002. Earth geography from 500 to 400 million years ago: A faunal and palaeomagnetic review. Journal of the Geological Society, 159: 631−644.

Cocks, L. R. M., Torsvik, T. H., 2007. Siberia, the wandering northern terrane, and its changing geography through the Paleozoic. Earth-Science Reviews, 82: 29−74.

Cogné, J. -P., Humler, E., 2006. Trends and rhythms in global seafloor generation rate. Geochemistry, Geophysics, Geosystems, 7: Q03011.

Cogné, J. -P., Humler, E., 2008. Global scale patterns of continental fragmentation: Wilson′s cycles as a constraint for long-term sea-level changes. Earth and Planetary Science Letters, 273: 251−259.

Cogné, J. -P., Humler, E., Courtillot, V., 2006. Mean age of oceanic lithosphere drives eustatic sea-level change since Pangea breakup. Earth and Planetary Science Letters, 245: 115−122.

Conrad, C. P., Lithgow-Bertelloni, C., 2002. How mantle slabs drive plate tectonics. Science, 298: 207−209.

Crowley, T. J., Burke, K. C., 1998. Tectonic boundary conditions for climate reconstructions. In: Charnock, H., Dewey, J. F., Conway Morris, S., Navrotsky, A., Oxburgh, E. R., Price, R. A., Skinner, B. J., (eds). Oxford monograph on geology and geophysics. New York: Oxford University Press, 285.

Dana, J. D., 1863. Manual of Geology. London: Theodore Bliss and Co.

d′Aubuisson de Voisins, J. F., 1819. Traité de Géognosie (nouvelle édition revue et corrigée). Strasbourg: Tome Premier.

DeMets, C., Gordon, R. G., Argus, D. F., Stein, S., 1990. Current plate motions. Geophysical Journal International, 101: 425−478.

DeMets, C., Gordon, R. G., Argus, D. F., Stein, S., 1994. Effect of recent revisions to the geomagnetic reversal time scale on estimates of current plate motions. Geophysical Research Letters, 21: 2191−2194.

Demicco, R. V., 2004. Modeling seafloor-spreading rates through time. Geology, 32: 485−488.

Dickins, J. M., 1993. Climate of the Late Devonian to Triassic. Palaeogeography, Palaeoclimatology, Palaeoecology, 100: 89−94.

Domeier, M., Torsvik, T., 2014. Plate tectonics in the late Paleozoic. Geoscience Frontiers, 5: 303−350.

Donovan, D. T., Jones, E. J. W., 1979. Causes of world-wide changes in sea level. Journal of the Geological Society, 136: 187−192.

Dromart, G., Garcia, J. P., Picard, S., Atrops, F., Lécuyer, C., Sheppard, S. M. F., 2003. Ice age at the Middle−Late Jurassic transition? Earth and Planetary Science Letters, 213: 205−220.

Engebretson, D. C., Kelley, K. P., Harold, J. C., Richards, M. A., 1992. 180 Million years of subduction. GSA Today, 2: 94−95.

Ferrari, O. M., Hochard, C., Stampfli, G. M., 2008. An alternative plate tectonic constrained model for the Paleozoic−Early Mesozoic Palaeotethyan evolution of southeast Asia, with special attention to northern Thailand. Tectonophysics, 451: 346−365.

Flores-Reyes, K. E., 2009. Mesozoic oceanic terranes of southern Central America —— Geology, geochmistry and geodynamics. Lausanne: Faculté des géosciences et de l′environnement, Université de Lausanne, 329.

Forsyth, D., Uyeda, S., 1975. On the relative importance of the driving forces of Plate Motion. Geophysical Journal of the Royal Astronomical Society, 43: 163−200.

Frakes, L. A., Francis, J. E., 1988. A guide to Phanerozoic cold polar climates from high-latitude ice-rafting in the Cretaceous. Nature, 333: 547−549.

Frakes, L. A., Francis, J. E., Syktus, J. I., 1992. Climate modes of the Phanerozoic. Cambridge: Cambridge University Press, ISBN: 0521366275.

Francois, L. M., Walker, J. C. G., 1992. Modelling the Phanerozoic carbon cycle and climate: Constraints from the $^{87}Sr/^{86}Sr$ isotopic ratio of seawater. American Journal of Science, 292: 81−135.

Gaffin, S., 1987. Ridge volume dependence on seafloor generation rate and inversion using long term sea level change. American Journal of Science, 287: 596−611.

Hafkenscheid, E., Wortel, M. J. R., Spakman, W., 2006. Subduction history of the Tethyan region derived from seismic tomography and tectonic reconstructions. Journal of Geophysical Research, 111: B08401.

Hallam, A., 1984. Pre-Quaternary sea-level changes. Annual Review of Earth and Planetary Sciences, 12: 205.

Haq, B. U., Schutter, S. R., 2008. A chronology of Paleozoic sea-level changes. Science, 322: 64−68.

Haq, B., Hardenbol, J., Vail, P. R., 1987. Chronology of fluctuating sea levels since the Triassic. Science, 235: 1156−1167.

Hays, J. D., Pitman, W. C., 1973. Lithospheric plate motion, sea level changes and climatic and ecological consequences. Nature, 246: 18−22.

Hochard, C., 2008. GIS and geodatabases application to global scale plate tectonics modeling. Lausanne: Faculté des géosciences et de l′environnement, Université de Lausanne, 164.

Howell, D. G., Jones, D. L., Schermer, E. R., 1985. Tectonostratigraphic terranes of the circum-Pacific region. Circum-Pacific Council for Energy and Mineral Resources. Earth Science Series, 1: 3−30.

Howell, D. G., 1995. Principles of terrane analysis: New Applications for Global Tectonics. 2nd Edition. London: Chapman and Hall, ISBN: 041254640X.

Humler, E., Langmuir, C., Daux, V., 1999. Depth versus age: New perspectives from the chemical compositions of ancient crust. Earth and Planetary Science Letters, 173: 7−23.

Keen, M. J., Klein, E. M., Melson, W. G., 1990. Ocean-ridge basalt compositions correlated with palaeobathymetry. Nature, 345: 423−426.

Kelvin, L., 1864. On the secular cooling of the Earth. Transaction of the Royal Society of Edinburgh, 23: 167−169.

Klein, E. M., Langmuir, C. H., 1987. Global correlations of ocean ridge basalt chemistry with axial depth and crustal thickness. Journal of Geophysical Research, 92: 8089−8115.

Kominz, M. A., 1984. Oceanic ridge volumes and sea-level change: An error analysis. AAPG Memoir, 36: 109−127.

Labrosse, S., Jaupart, C., 2007. Thermal evolution of the Earth: Secular changes and fluctuations of plate characteristics. Earth and Planetary Science Letters, 260: 465−481.

Larson, R. L., 1991. Latest pulse of Earth: Evidence for a mid-Cretaceous superplume. Geology, 19: 547−550.

Lasaga, A. C., Berner, R. A., Garrels, R. M., 1985. An improved geochemical model of atmospheric CO_2 fluctuations over the past 100 million years. In: Union, A. G., (ed). Chapman Conference on Natural Variations in Carbon Dioxide and the Carbon Cycle, Tarpon Springs, FL, United States, 397−411.

Le Grand, H. E., 2002. Plate tectonics, terranes and continental geology. In: Oldroyd, D. R., (ed). The Earth inside and out; some major contributions to geology in the twentieth century. London: Geological Society of London, 199−213.

Li, Z. -X., Powell, C., 2001. An outline of the palaeogeographic evolution of the Australasian region since the beginning of the Neoproterozoic. Earth Science Reviews, 53: 237−277.

McElhinny, M. W., Powell, C., Pisarevsky, S., 2003. Paleozoic terranes of eastern Australia and the drift history of Gondwana. Tectonophysics, 362: 41−65.

McKenzie, D. P., 1977. Initiation of trenches: A finite amplitude instability. In: Talwani, M., Pittman, W. C., (eds). Island Arcs, Deep Sea Trenches and Back-Arc Basins. Washington: American Geophysical Union, 57−62.

Miller, K. G., Kominz, M. A., Browning, J. V., Wright, J. D., Mountain, G. S., Katz, M. E., Sugarman, P. J., Cramer, B. S., Christie-Blick, N., Pekar, S. F., 2005. The Phanerozoic record of global sea-level change. Science, 310: 1293−1298.

Moix, P., Beccaletto, L., Kozur, H. W., Hochard, C., Rosselet, F., Stampfli, G. M., 2008. A new classification of the Turkish terranes and sutures and its implication for the Palaeotectonic history of the region. In: Sorkhabi, R., Heydari, E., (eds). Asia out of the Tethys: Geochronologic, Tectonic and Sedimentary Records. Tectonophysics, 7−39.

Mueller, S., Phillips, R. J., 1991. On the initiation of subduction. Journal of Geophysical Research, 96: 651−665.

Müller, R. D., Roest, W. R., Royer, J. -Y., 1998. Asymmetric sea-floor spreading caused by ridge-plume interactions. Nature, 396: 455−459.

Müller, R. D., Sdrolias, M., Gaina, C., Roest, W. R., 2008a. Age, spreading rates, and spreading asymmetry of the world′s ocean crust. Geochemistry, Geophysics, Geosystems, 9: 18−36.

Müller, R. D., Sdrolias, M., Gaina, C., Steinberger, B., Heine, C., 2008b. Long-term sea-level fluctuations driven by ocean basin dynamics. Science, 319: 1357−1362.

Niu, Y., Hekinian, R., 1997. Spreading-rate dependence of the extent of mantle melting beneath ocean ridges. Nature, 385: 326−329.

Parai, R., Mukhopadhyay, S., 2012. How large is the subducted water flux? New constraints on mantle regassing rates. Earth and Planetary Science Letters, 317−318: 396−406.

Parsons, B., 1982. Causes and consequences of the relation between area and age of the ocean floor. Journal of Geophysical Research, 87: 289−302.

Parsons, B., Sclater, J. G., 1977. An analysis of the variation of ocean floor bathymetry and heat flow with age. Journal of Geophysical Research, 82: 803−827.

Prokoph, A., Shields, G. A., Veizer, J., 2008. Compilation and time-series analysis of a marine carbonate $\delta^{18}O$, $\delta^{13}C$, $^{87}Sr/^{86}Sr$ and $\delta^{34}S$ database through Earth history. Earth-Science Reviews, 87: 113−133.

Ross, C. A., Ross, J. R. P., 1988. Late Paleozoic transgressive-regressive deposition. Society of Economic Palaeontologists and Mineralogists Special Publication, 42: 227−247.

Rowley, D. B., 2002. Rate of plate creation and destruction: 180 Ma to present. GSA Bulletin, 114: 927−933.

Royer, D. L., 2006. CO_2-forced climate thresholds during the Phanerozoic. Geochimica et Cosmochimica Acta, 70: 5665−5675.

Royer, D. L., Berner, R. A., Montanez, I. P., Tabor, N. J., Beerling, D. J., 2004. CO_2 as a primary driver of Phanerozoic climate. GSA Today, 14: 4−10.

Saltzman, M. R., Young, S. A., 2005. Long-lived glaciation in the Late Ordovician? Isotopic and sequence-stratigraphic evidence from western Laurentia. Geology, 33: 109−112.

Schardt, H., 1893. Sur l'origine des Préalpes romandes. Archives de physique et des sciences naturelles de Genève, 3: 570−583.

Schellart, W. P., Freeman, J., Stegman, D. R., Moresi, L., May, D., 2007. Evolution and diversity of subduction zones controlled by slab width. Nature, 446: 308−311.

Schmidt, P., Powell, C., Li, Z. -X., Thrupp, G., 1990. Reliability of Paleozoic palaeomagnetic poles and APWP of Gondwanaland. In: Schmidt, P., Van de Voo, R., (eds). Reliability of Palaeomagnetic Data. Tectonophysics, 87−100.

Scotese, C. R., Barrett, S. F., 1990. Gondwana′s movement over the South Pole during the Paleozoic: Evidence from lithological indcators of climate. In: McKerrow, W. S., Scotese, C. R., (eds). Paleozoic Palaeogeography and Biogeogrpahy. The Geological Society, 75−85.

Scotese, C. R., Boucot, A. J., McKerrow, W. S., 1999. Gondwanan palaeogeography and palaeoclimatology. Jounal of African Earth Sciences, 28: 99−114.

Sengör, A. M. C., Dewey, F. R. S., Robertson, A. H. F., 1990. Terranology: Vice or Virtue? Philosophical Transactions of the Royal Society of London, A331: 457−477.

Small, C., Danyushevsky, L. V., 2003. Plate-kinematic explanation for mid-oceanic-ridge depth discontinuities. Geology, 31: 399−402.

Stampfli, G. M., 1993. Le Briançonnais, terrain exotique dans les Alpes? Eclogae Geologicae Helvetiae, 86: 1−45.

Stampfli, G. M., 2000. Tethyan oceans. Geological Society, London, Special Publications, 173: 1−23.

Stampfli, G. M., Borel, G. D., 2002. A plate tectonic model for the Paleozoic and Mesozoic constrained by dynamic plate boundaries and restored synthetic oceanic isochrons. Earth and Planetary Science Letters, 196: 17−33.

Stampfli, G. M., Borel, G. D., 2004. The TRANSMED transects in space and time: Constraints on the palaeotectonic evolution of the Mediterranean domain. In: Cavazza, W., Roure, F., Spakman, W., Stampfli, G. M., Ziegler, P., (eds). The TRANSMED Atlas: The Mediterranean Region from Crust to Mantle. Springer Verlag, 53−80.

Stampfli, G. M., Borel, G., Marchant, R., Mosar, J., 2002a. Western Alps geological constraints on western Tethyan reconstructions. In: Rosenbaum, G., Lister, G. S., (eds). Reconstruction of the evolution of the Alpine-Himalayan Orogen, 75−104.

Stampfli, G. M., Hochard, C., 2009. Plate tectonics of the Alpine realm. Geological Society, London, Special Publications, 327: 89−111.

Stampfli, G. M., Hochard, C., Vérard, C., Wilhem, C., von Raumer, J., 2013. The formation of Pangea. Tectonophysics, 593: 1−19.

Stampfli, G. M., Kozur, H. W., 2006. Europe from the Variscan to the Alpine cycles. Geological Society, London, Memoirs, 32: 57−82.

Stampfli, G. M., Marcoux, J., Baud, A., 1991. Tethyan margins in space and time. In: Channell, J. E. T., Winterer, E. L., Jansa, L. F., (eds). Palaeogeography and Palaeoceanography of Tethys. Palaeogeography, Palaeoclimatology, Palaeoecology, 373−410.

Stampfli, G. M., Mosar, J., Favre, P., Pillevuit, A., Vannay, J. -C., 2001. Permo-Mesozoic evolution of the western Tethys realm: The Neo-Tethys East Mediterranean Basin connection. Anglais, 186: 51−108.

Stampfli, G. M., Mosar, J., Marquer, D., Marchant, R., Baudin, T., Borel, G., 1998. Subduction and obduction processes in the Swiss Alps. Tectonophysics, 296: 159−204.

Stampfli, G. M., Pillevuit, A., 1993. An alternative Permo-Triassic reconstruction of the kinematics of the Tethyan realm. In: Dercourt, J., Ricou, L. -E., Vrielinck, B., (eds). Atlas Tethys Palaeoenvironmental Maps. Paris: Gauthier-Villars, 55−62.

Stampfli, G. M., Vavassis, I., De Bono, A., Rosselet, F., Matti, B., Bellini, M., 2003. Remnants of the Palaeotethys oceanic suture-zone in the western Tethyan area. Bollettino della Società Geologica Italiana e del Servizio Geologico d′Italia Volume special, 2: 1−23.

Stampfli, G. M., von Raumer, J. F., Borel, G. D., 2002b. Paleozoic evolution of pre-Variscan terranes: From Gondwana to the Variscan collision. GSA Special Papers, 364: 263−280.

Stampfli, G. M., von Raumer, J. F., Wilhem, C., 2011. The distribution of Gondwana-derived terranes in the early Paleozoic. In: Gutiérerrez-Marco, J. C., Rabano, I., Garcia-Bellido, D., (eds). Ordovician of the World. Madrid: Instituto Geológico y Minero de España, 567−574.

Stein, C. A., Stein, S., 1992. A model for the global variation in oceanic depth and heat flow with lithospheric age. Nature, 359: 123−129.

Stern, R. J., 2004. Subduction initiation: Spontaneous and induced.

Earth and Planetary Science Letters, 226: 275−292.

Suan, G., Mattioli, E., Pittet, B., Lécuyer, C., Suchéras-Marx, B., Duarte, L. V., Philippe, M., Reggiani, L., Martineau, F., 2010. Secular environmental precursors to Early Toarcian (Jurassic) extreme climate changes. Earth and Planetary Science Letters, 290: 448−458.

Tardy, Y., N′Kounkou, R., Probst, J. -L., 1989. The global water cycle and continental erosion during Phanerozoic time (570 my). American Journal of Science, 289: 455−483.

Torsvik, T. H., Cocks, L. R. M., 2005. Norway in space and time: A centennial cavalcade. Norwegian Journal of Geology, 85: 73−86.

Torsvik, T. H., Müller, R. D., van der Voo, R., Steinberger, B., Gaina, C., 2008. Global plate motion frames: Toward a unified model. Reviews of Geophysics, 46: 1−44.

Torsvik, T. H., Smethurst, M. A., Meert, J. G., van der Voo, R., McKerrow, W. S., Brasier, M. D., Sturt, B. A., Walderhaug, H. J., 1996. Continental break-up and collision in the Neoproterozoic and Paleozoic —— A tale of Baltica and Laurentia. Earth-Science Reviews, 40: 229−258.

Torsvik, T. H., van der Voo, R., 2002. Refining Gondwana and Pangea palaeogeography: Estimates of Phanerozoic non-dipole (octupole) fields. Geophysical Journal International, 151: 771−794.

Turcotte, D. L., 1980. On the thermal evolution of the earth. Earth and Planetary Science Letters, 48: 53−58.

Turcotte, D. L., Schubert, G., 2002. Geodynamics. 2nd Edition. Cambridge: Cambridge University Press.

Urey, H. C., 1952. The Planets: Their Origin and Development. New Haven: Yale University Press.

Vail, P. R., Mitchum, R. M., Thompson, S., 1977. Seismic stratigraphy and changes of sea level. In: Payton, C. E., (ed). Seismic stratigraphy —— Applications to hydrocarbon exploration. Tulsa: AAPG memoir, 26: 83−98.

Veizer, J., Ala, D., Azmy, K., Bruckschen, P., Buhl, D., Bruhn, F., Carden, G. A. F., Diener, A., Ebneth, S., Godderis, Y., Jasper, T., Korte, C., Pawellek, F., Podlaha, O. G., Strauss, H., 1999. $^{87}Sr/^{86}Sr$, $\delta^{13}C$ and $\delta^{18}O$ evolution of Phanerozoic seawater. Chemical Geology, 161: 59−88.

Vérard, C., Flores-Reyes, K., Stampfli, G., 2012. Geodynamic reconstructions of the South America−Antarctica plate system. Journal of Geodynamics, 53: 43−60.

Vérard, C., Hocahrd, C., Stampfli, G. M., 2012. Non-random distribution of Euler poles: Is plate tectonics subject to rotational effets? Terra Nova, 24: 467−476.

Vérard, C., Hochard, C., Baumgartner, P. O., 2011. Geodynamic evolution of the Earth over 600 Ma: Palaeo-topography and palaeo-bathymetry (from 2D to 3D). San Francisco: American Geophysical Union Fall Meeting.

Vérard, C., Hochard, C., Baumgartner, P. O., Stampfli, G. M., 2015. 3D palaeogeographic reconstructions of the Phanerozoic versus sea-level and Sr-ratio variations. Journal of Palaeogeography, 4: 64−84.

Vérard, C., Stampfli, G. M., 2013a. Geodynamic Reconstructions of the Australides 1: Paleozoic. Geosciences, 3: 311−330.

Vérard, C., Stampfli, G. M., 2013b. Geodynamic Reconstructions of the Australides 2: Mesozoic−Cainozoic. Geosciences, 3: 331−353.

von Raumer, J. F., Bussy, F., Stampfli, G. M., 2009. The Variscan evolution in the External massifs of the Alps and place in their Variscan framework. Comptes Rendus Geoscience, 341: 239−252.

von Raumer, J. F., Stampfli, G. M., 2008. The birth of the Rheic Ocean —— Early Paleozoic subsidence patterns and subsequent tectonic plate scenarios. Tectonophysics, 461: 9−20.

von Raumer, J., Bussy, F., Schaltegger, U., Schaltegger, U., Schulz, B., Stampfli, G. M., 2013. Pre-Mesozoic Alpine basements —— Their place in the European Paleozoic framework. GSA Bulletin, 125: 89−108.

von Raumer, J., Stampfli, G., Hochard, C., Gutierrez-Marco, C. J., 2006. The Early Paleozoic in Iberia a plate-tectonic interpretation. Zeitschrift der Deutschen Gesellschaft für Geowissenschaften, 157: 575−584.

Wallmann, K., 2001. Controls on the Cretaceous and Cenozoic evolution of seawater composition, atmospheric CO_2 and climate. Geochimica et Cosmochimica Acta, 65: 3005−3025.

Wallmann, K., 2004. Impact of atmospheric CO_2 and galactic cosmic radiation on Phanerozoic climate change and the marine $\delta^{18}O$ record. Geochemistry, Geophysics, Geosystems, 5: Q06004.

Webb, P. J., 2012. Mantle circulation models: Constraining mantle dynamics, testing plate motion history and calculating dynamic topography. Cardiff: University of Cardiff, 256.

Wilhem, C., 2010. Plate Tectonics of the Altaids. Lausanne: Faculté des géosciences et de l′environnement. Université de Lausanne, 347.

Zhong, S., Gurnis, M., 1995. Mantle convection with plates and mobile. Faulted Plate Margins Science, 267: 838−843.

(Edited by Min Liu)